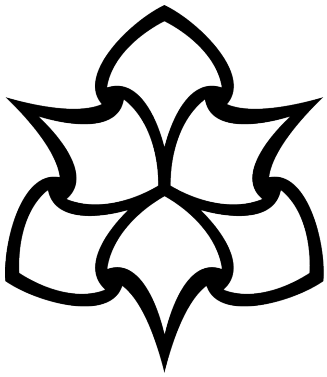

Numerical investigation of piston-modal wave resonance in the narrow gap formed by a box in front of a wall

Sheng-Chao JIANG (姜胜超),[1, 2, a)] Wei BAI (柏威),[3] and Guo-Qiang TANG (唐国强)[2]
[1)] *School of Naval Architecture, State Key Laboratory of Structural Analysis for Industrial Equipment, Dalian University of Technology, Dalian 116024, China*
[2)] *State Key Laboratory of Coastal and Offshore Engineering, Dalian University of Technology, Dalian 116024, China*
[3)] *School of Computing, Mathematics and Digital Technology, Manchester Metropolitan University, Chester Street, Manchester M1 5GD, UK*

(Dated: 15 April 2019)

Piston-modal wave resonance between a ship section and a bottom mounted terminal is studied by employing a numerical wave flume based on OpenFOAM® package. A systematic investigation on the piston-modal behavior is performed to characterize the influence of fluid viscosity and flow rotation. Around the resonant frequency, the fluid viscosity and flow rotation not only dissipate the wave amplitude in the narrow gap, but also increase the wave amplitude in the upstream of the box. The dynamic mechanism behind the phenomenon is found to be the interaction between the energy dissipation induced by the fluid vortical flow and energy transformation associated with free surface motion. The increased incident wave amplitude can cause the normalized wave amplitudes and wave forces to deviate more from the potential flow results; while the variation of reflection coefficient is dependent on box-wall geometries. All of these phenomena imply more significant effect of fluid viscosity and flow rotation with the increase of incident wave amplitude, but the energy dissipation is not the only factor in piston-modal resonance.

In this work, we evaluated wave resonance in the narrow gap formed by a ship section in front of a wall. The focus of this study is to examine the interaction between the energy dissipation induced by the fluid vortical flow and energy transformation associated with free surface motion, by which some dynamic mechanisms of gap resonance can be revealed.

I. INTRODUCTION

In the last two decades, the topic of resonant fluid motion within a vertical gap between multiple bodies in close proximity has been receiving increasing attentions. Being exposed to incident wave actions, the fluid inside the narrow gap may perform considerable free surface oscillations and lead to extremely large wave forces on the vessels. This is a key technical challenge for the safety of a Liquefied Natural Gas (LNG) carrier or shuttle oil tanker alongside a Floating Liquefied Natural Gas (FLNG) or in front of an offshore terminal for loading and offloading operations. Similar phenomena may also happen in the fluid resonance within a moonpool or the ship in front of a gravity wharf. Therefore, understanding the fundamental physics in the resonant fluid flows is important to the marine operation and structure safety.

The appearance condition of the fluid resonance in the narrow gap can be estimated roughly according to the natural frequency of fluid bulk involved in the oscillation. In this sense, the resonant mode in the narrow gap can be considered as the eigenvalue of the corresponding boundary value problem, where the resonant frequency and associated free surface shape are the eigenfrequency and eigenvector, respectively. An analytical solution for the gap resonance problem was derived in Molin (2001), where the formulae for the piston- and sloshing-modal shapes and the corresponding frequencies were obtained via solving an eigenvalue equation. Zhang and Bandyk (2013) proposed an eigenfunction matching approach for solving the fluid resonance in a narrow gap between two heaving rectangular boxes in a two-layer fluid flow. Sun, Eatock Taylor, and Taylor (2015) simulated the lateral piston- and longitudinal sloshing-modal resonant behavior in the closely spaced vessels, in which the first and second-order wave diffraction models were adopted in the frequency domain. Ren, Wu, and Thomas (2016) and Li, Shi, and Wu (2017) analyzed the wave excited motion of a body floating on water confined and wide polynya between two semi-infinite elastic ice sheets, respectively, where natural frequencies of body motion and the subsequent resonances in both coupled and uncoupled motions are investigated. Extensive comparisons demonstrated that the potential flow model is capable of predicting the resonant frequency, unfortunately, the resonant amplitude is also reported to be over-estimated compared to the laboratory observations, such as in Saitoh, Miao, and Ishida (2006); Faltinsen, Rognebakke, and Timokha (2007); Peric and Swan (2015) and among others. Many approximations were developed to hold the exaggerated resonant amplitude back to a realistic level based on the introduction of artificial damping in the potential flow model. Newman (2004) and Chen (2004) applied the flexible lid condition and the dissipative term into the free surface condition in the narrow gap, respectively. Liu and Li (2014) analysed a linear semi-analytical solution for the gap resonance problem, where the dissipative boundary conditions (Liu *et al.*, 2008) were imposed on both the free surface in the narrow gap and the fluid domain below the barges. A time-domain potential flow solver was de-

[a)] Electronic mail: jiangshengchao@foxmail.com

veloped by Ning *et al.* (2015, 2018), in which the artificial viscous coefficient was imposed on the fully nonlinear free surface condition in the narrow gap. Based on the calibration of the artificial viscous coefficient by their laboratory tests, numerical results can agree well with the experimental data.

There are two important issues of concern in applications of the potential flow model with artificial damping method. One is that the value of artificial damping has to be calibrated according to the experimental data, leading to that the numerical work is effective only after the laboratory observations. The other is the actual mechanical essence behind the resonant phenomenon in fact still cannot be simulated correctly. It has been reported in Lu *et al.* (2011a) and Lu *et al.* (2011b) that different artificial damping values have to be adopted for the wave response in the narrow gap and wave forces on the boxes, separately, even for the same structures under the same waves. This is the inherent drawback of the modified potential flow model. It is speculated that the artificial damping should be closely relevant to the fluid viscosity and energy dissipation neglected by the potential flow model. A variety of investigations were carried out for understanding the fundamental physics of vortical flow and eddy motion in the resonant response, which can give us a deep insight into the mechanism of piston-modal resonance. Lu *et al.* (2010) examined the gap resonance problem by using a finite element based Navier-Stokes solver with CLEAR-VOF method (Computational Lagrangian-Eulerian Advection Remap VOF Method). Kristiansen and Faltinsen (2010) studied the ship motion near a bottom-mounted terminal under the wave action according to an inviscid vortex tracking method. Numerical results indicated that majority of energy dissipation occurs in the vicinity of gap entrance. The experimental and numerical investigation by Fredriksen, Kristiansen, and Faltinsen (2014) suggested that the large-amplitude piston-type free surface oscillation in the moonpool is significantly dependent on the moonpool edge profiles and heaving amplitudes. Similar physical phenomena can also be found in Moradi, Zhou, and Cheng (2015) for the gap resonance problem, where the significant effect of gap inlet configurations (i.e. sharp and curved corners) on the resonant wave frequencies and amplitudes can be observed. Feng *et al.* (2017) investigated a three-dimensional gap resonance between two side-by-side barges, where a close examination of flow velocity and vorticity in the gap region was conducted for revealing the damping mechanism at the piston mode. All these works confirm that the energy dissipation induced by flow separation and vortex motion, especially in the vicinity of the gap bottom, has the significant effect on the wave responses in the narrow gap.

Besides the energy dissipation, other hydrodynamic behavior due to the large-amplitude free surface response has also been paid more attention, recently. Feng and Bai (2015) investigated the influence of free surface nonlinearity on the three-dimensional wave resonance between two side-by-side barges by using a fully nonlinear potential flow model. Harmonic analysis illustrated that the resonant frequency slightly shifts to higher values as incident wave steepness increases, equivalent to a stiff spring in a nonlinear mass-spring system. An experiment of the resonant fluid response between two identical fixed rectangular boxes was conducted by Zhao *et al.* (2017). The higher-order harmonic components were separated and the nonlinear wave-wave and wave-structure interactions were investigated under the NewWave-type transient wave groups. Zhao, Hu, and Chen (2017) considered the hydrodynamic behavior between side-by-side barges but with connections. Huang *et al.* (2018) studied the response of passive telescopic gangway between monohull flotel and FPSO (Floating Production Storage and Offloading) in non-parallel side-by-side configurations. Laboratory observations showed that the resonant fluid motion can lead to more complex dynamic response properties, including the impact of multi-body hydrodynamic interaction and the transient snap loading response of hawsers, and so on. Bonfiglio and Brizzolara (2018) described the near field flow characteristics around a catamaran cross section at the resonant condition. The free surface nonlinearity due to high oscillation amplitudes and resonant free surface motions was addressed, including the energetic vortex shedding and steep wave action. The wave resonance in the narrow gap between two non-identical side-by-side boxes were investigated by Jiang, Bai, and Tang (2018); Jiang *et al.* (2019). Numerical simulations suggested that the energy transformation due to the large-amplitude free surface response also plays an important role during the process of resonant oscillations, in addition to the energy dissipation in the narrow gap. However, the interaction between the energy dissipation and energy transformation is still lack of comprehensive investigation, which is expected to improve the understanding of related phenomena involved in the gap resonance problem.

The main objective of this study is to promote a deep understanding on the influence of fluid viscosity and flow rotation on the behavior of piston-modal wave resonance. According to the above-mentioned research, we can observe that the previous work mainly focused on the study of two-box system. No much light was thrown on the gap resonance formed by a ship section in front of a vertical wall, which is also a typical marine operation such as the alongside arrangement between a LNG carrier and a bottom mounted terminal. As the box-wall system can lead to a full reflection phenomenon under the wave action, the stronger large-amplitude free surface oscillation and other more complex dynamic response are expected. The present study will shed light upon the physics of this problem. Numerical results include the wave responses in the narrow gap and in the upstream of the box, the horizontal and vertical wave forces on the box, and the reflection coefficient of the box-wall system. The interaction between the energy dissipation and energy transformation is addressed by varying incident amplitudes and box-wall geometries, especially when the resonance happens. The near field flow pattern is also presented aiming to characterize the vortex shedding and eddy motion in the gap region, which is helpful for understanding the dissipative mechanism in a realistic fluid. In summary, numerical analysis of piston-modal wave resonance is carried out under various influencing factors, by which the influence of fluid viscosity and flow rotation can be revealed from the perspective of energy dissipation and energy transformation.

II. MATHEMATICAL FORMULATION

The viscous fluid flow model for incompressible two-phase flows based on Navier-Stokes equations is adopted for numerical simulations. In the Eulerian reference system, the governing equations for the mass and momentum conservations can be given as,

$$\frac{\partial \rho}{\partial t} + \frac{\partial \rho u_i}{\partial x_i} = 0 \tag{1a}$$

$$\frac{\partial \rho u_i}{\partial t} + \frac{\partial \rho u_i u_j}{\partial x_j} = \rho g_i - \frac{\partial p}{\partial x_i} + \mu \frac{\partial}{\partial x_j}\left(\frac{\partial u_i}{\partial x_j} + \frac{\partial u_j}{\partial x_i}\right) \tag{1b}$$

where u_i is the fluid velocity, p is the dynamic pressure, and the Cartesian tensor notation is used here. ρ and μ are the fluid density and fluid dynamic viscosity, respectively; and g_i is the gravitational acceleration.

The above equations are solved for both air and water simultaneously, and the fluid is tracked using the scalar field φ which is 0 for air and 1 for water. Any intermediate value between 0 and 1 represents a mixture of air and water. In the Volume of Fluid (VOF) method (Hirt and Nichols, 1981), the distribution of the fraction indicator φ is modeled by an advection equation,

$$\frac{\partial \varphi}{\partial t} + \frac{\partial \varphi u_i}{\partial x_i} + \frac{\partial \varphi(1-\varphi)u_{ir}}{\partial x_i} = 0 \tag{2}$$

where u_{ir} is the relative velocity of the phases. The last term on the left hand side of Eq. (2) is for compression, which has been demonstrated to limit the smearing of the interface(Afshar, 2010; Rusche, 2003). In numerical simulations, the contour of VOF function with $\varphi = 0.50$ is used to represent the interface between the water and air phases. The spatial variation of fluid density and dynamic viscosity can be expressed through the weighting as follows,

$$\rho = \varphi\rho_W + (1-\varphi)\rho_A, \tag{3a}$$

$$\mu = \varphi\mu_W + (1-\varphi)\mu_A, \tag{3b}$$

where the subscripts W and A represent the Water phase and Air phase, respectively.

The toolbox 'waves2Foam' is utilized to generate the incident wave and avoid the internal wave reflection, where a relaxation zone is defined at the inlet boundary of the numerical wave flume. The exponential relaxation function

$$\alpha_R(\chi_R) = 1 - \frac{\exp(\chi_R^{3.5}) - 1}{\exp(1) - 1} \quad \chi_R \in [0,1] \tag{4}$$

is applied within the relaxation zone,

$$\vartheta = \alpha_R \vartheta_C + (1-\alpha_R)\vartheta_T, \tag{5}$$

where ϑ is either the velocity u_i or volume fraction of water φ, and the subscripts C and T represent the Computed value and Target value, respectively. The definition of α_R is the same as in Fuhrman, Madsen, and Bingham (2006), where α_R in Eq. (4) is only activate in the relaxation zone, and it is always 1 at the interface between the non-relaxed part of the computational domain. Detailed information about the relaxation technique can be found in Mayer *et al.* (1998), Engsig-Karup (2006) and Jacobsen, Fuhrman, and Fredsøe (2012).

The governing equations (1a)-(1b) and the advection transport equation (2) are solved based on the Finite Volume Method (FVM) integrated in the OpenFOAM® package. The velocity and pressure are decoupled by the PISO (Pressure Implicit with Splitting of Operators) algorithm (Issa, 1986). The Courant-Friedrichs-Lewy (CFL) condition is adopted to determine the time increment automatically, where the largest allowed Courant Number is set to $C_r = 0.2$. The numerical computations always start from the still state, which means the zero velocity and hydrostatic pressure are specified as the initial conditions. At the inlet boundary, the vector is defined as that of a sinusoidal incident wave and the gradient of pressure is set to zero. The no-slip boundary condition is imposed at the solid wall including the body surface, seabed and vertical wall. At the upper boundary of the numerical wave flume, the Dirichlet and Neumann types of boundary conditions are prescribed to the pressure and velocity respectively. In this study, the interface tension between the air and water phases is neglected since the dynamic effects from the air phase are very small. For the details of numerical implements in OpenFOAM®, the readers may refer to Jasak (1996) and Rusche (2003).

Finally, it should be mentioned that the classical linear potential flow model is also adopted in this study for the purpose of comparison, for which the theoretical formulation is omitted here, as it is well known in many textbooks (Newman, 1977; Mei, 1989; Faltinsen, 1993).

III. NUMERICAL SETUP

Fig. 1 shows the definition sketch of the coordinate system, which is defined in such a way that the origin is located at the still water level, and x-axis is in the wave propagation direction and y-axis is in the upward direction. The ship section is considered as a simple rectangular shape cross-section in the present study, defined as Box with the breadth B and the draft D in the finite water depth h. In present work, only the fixed box in front of a wall is considered. A narrow gap with the breadth B_g is formed by the box and the wall, where the extremely large amplitude of fluid resonance can be observed as the incident wave frequency is close to the natural frequency of the confined fluid bulk. The box breadth B = 0.50 m and water depth h = 0.50 m are adopted in all the cases, and the corresponding values for other parameters are designed to conduct the intended investigation. In numerical simulations, three gap breadths B_g = 0.050 m, 0.070 m, 0.090 m and three box drafts D = 0.153 m, 0.252 m, 0.350 m, together with four incident wave amplitudes A_i = 0.004 m, 0.008 m, 0.012 m, 0.016 m are selected, so totally 27 cases are considered. The detailed comparison and analysis among the numerical results

are helpful to examine the hydrodynamic behavior of piston-modal resonance, including the wave amplitudes A_g and A_u in the narrow gap and in the upstream of the box, the horizontal and vertical wave forces F_h and F_v, and the reflection coefficient K_r.

In the present study the height of the numerical wave flume is fixed at 0.8 m, and the length is changing in accordance with the incident wave length L for different simulations. A relaxation zone is arranged on the left side of the wave flume, which is around 3.0 - 5.0 L long; and the total length of the wave flume is around 10 - 15 L long. Four wave gauges, G1 - G4, are equipped to record the free surface elevation, as shown in Fig. 1. G1 is located in the middle of the gap for recording the wave response in the narrow gap; while G4 is situated in the upstream of the box, which is 0.005 m from the vertical wall of the box. G2 and G3 are located 1.5 L from the left side of the box for separating the incident and reflected waves, in which the distance between them is kept at 0.25 L.

IV. NUMERICAL VALIDATION AND MODEL TEST

In order to check the dependence of the simulation results on the mesh density, numerical simulations are carried out by using four different meshes for three configurations (see Tab. I), these are, $D = 0.252$ m with $B_g = 0.050$ m, 0.070 m, 0.090 m, respectively. As shown in Fig. 2, non-uniform meshes are adopted to discretise the computational domain for saving computational cost. The square fine meshes with high resolution are adopted around the box, especially in the vicinity of the narrow gap, to accurately capture the large-amplitude free surface oscillation and to account for the boundary layer effect. The rectangular meshes with intermediate resolution are adopted in the other computational domain, including the relaxation zone of generating the incident wave and the path of wave propagation. The largest aspect ratio is 1/2 (height/length) in the present numerical simulations. Typical mesh partitions in the vicinity of the box-wall system are depicted in Fig. 2, which corresponds to Mesh 1 in Tab. I.

For the purpose of illustration, the geometry of $D = 0.252$ m with $B_g = 0.050$ m is adopted for the mesh resolution test. The typical evolutions of the free surface oscillation $\eta(t)$ in the narrow gap measured at wave gauge G1 and the horizontal and vertical wave forces on the box with various mesh resolutions are depicted in Fig. 3, where the incident wave amplitude $A_i = 0.012$ m with the resonant frequency $\omega = 4.80$ rad/s is adopted as the incident wave condition. After a short transient period, clear steady-state evolutions can be observed after $t = 30$ s, indicating satisfactory performance of the relaxation zone in generating and eliminating the incident and reflection waves, respectively. Numerical simulations also suggest that very little discrepancy between the steady-state results of Mesh 3 and Mesh 4 can be observed, implying that the convergent solutions can be produced by Mesh 3.

Furthermore, the features of free surface oscillation in the narrow gap and wave forces on the box can also be observed according to the steady-state evolutions. As shown in Fig. 3a, numerical simulations suggest that the time signal of free surface oscillation is quite symmetric, and looks like a sinusoidal function. The time history of normalized free surface evolutions during 100 - 300 seconds by Mesh 3 is adopted for the Fourier analysis. Fig. 4a depicts that the dominating harmonic of wave elevations is at the incident wave frequency ω, confirming the insignificant effect of free surface nonlinearity on the large-amplitude piston-modal resonance. Similar behavior can also be observed in Figs. 3b and 4b, indicating the influence of wave nonlinearity is also negligible for horizontal wave forces on the box. In difference to free surface oscillations and horizontal wave forces, the vertical wave forces show the non-sinusoidal characteristics in Fig. 3c. The wave frequency spectra of vertical wave forces involve four frequencies in Fig. 4c, including the steady zero frequency term, the linear term, the 2nd-order double frequency term and even the small third-order triple frequency term. The linear component is the largest, but the other components are also non-negligible in behavior of vertical wave forces. Referring to the Bernoulli equation, the vertical wave forces should be closely relevant to the square of flow velocity under the box bottom, which is the main reason for the resultant nonlinearity.

The normalized free surface amplitudes in the narrow gap A_g/A_i at wave gauge G1 and the wave forces F_h and F_v on the box around the resonant frequency with four different mesh schemes are compared in Fig. 5. The resonant frequencies for different geometries are obtained by the conventional potential flow model, which have been tabulated in Tab. I. According to the averaged values of the crest and trough between the duration of 100 - 200 seconds, the amplitudes of free surface oscillation, horizontal and vertical wave forces can be computed, defined as A_g, F_h and F_v, respectively. The sensitivity analysis by varying the time window from the duration of 100 - 200 to 200 - 300 seconds shows the negligible effect on the amplitudes, indicating the steady states have been reached after $t = 100$ s. The comparisons in Fig. 5 show that the variation of mesh density has little effect on the amplitudes of free surface and wave forces if the number of cells exceeds 3×10^5. Again, Mesh 3 is able to produce convergent solutions, and hence it is adopted as the baseline for the following numerical investigations.

Numerical validations of wave amplitudes in the narrow gap are performed against the available laboratory test results in Tan *et al.* (2014) and the linear potential flow solutions. The mean normalized wave amplitudes A_g/A_i at wave gauge G1 are compared in Fig. 6, where the incident wave amplitudes is set at $A_i = 0.012$ m and measured at wave gauges G2 and G3. The numerical results at non-resonant conditions agree better with experiments than those at the resonant condition. Around the resonant frequency, the vorticity created at the sharp edge is more likely to generate the turbulent mixing. This might be the reason for the slight over-prediction in the present viscous fluid flow model around the resonant frequency. General speaking, the present numerical results are in agreement with the experimental measurements, indicating that the present numerical wave flume can work well in predicting wave responses. Nevertheless, the linear potential flow model over-predicts the wave amplitude around the

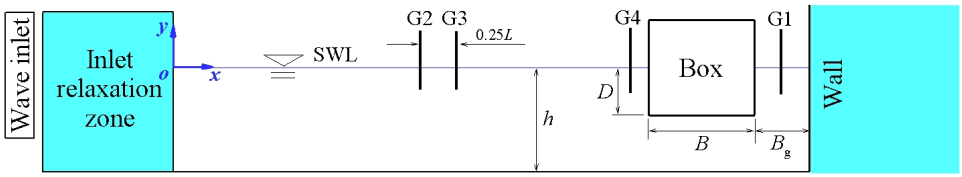

FIG. 1: Sketch of the definition of the numerical wave flume

TABLE I: Mesh information for convergent tests (Elements/Nodes)

D (m)	B_g (m)	ω_g	Mesh1	Mesh2	Mesh3	Mesh4
0.252	0.050	4.8 rad/s	79963/161820	232882/469330	343980/692378	471404/948064
0.252	0.070	4.5 rad/s	80317/162534	233914/471406	343868/692168	471411/948094
0.252	0.090	4.3 rad/s	82899/167752	243546/490782	358008/720588	490815/987070

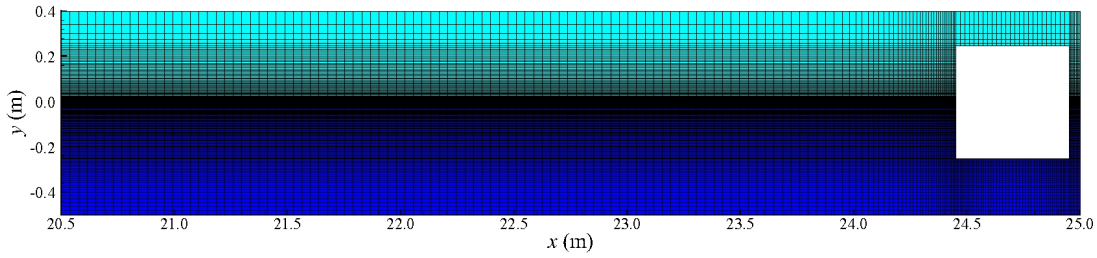

FIG. 2: Typical computational meshes in the vicinity of the box-wall system for the configuration of B_g = 0.050 m and D = 0.252 m

resonant frequency, demonstrating the indispensable of viscous fluid flow model. The amplitudes of the first three wave harmonic components are also included in Fig. 6, which can be obtained by using the bandpass filtering operation. Agreement between the original and filtered wave amplitudes confirms that the first-order wave component dominates the free surface oscillation in the narrow gap. The higher-order wave components of free surface elevation are remarkably smaller than the first-order component, implying the insignificant effect of free surface nonlinearity.

The numerical results of reflection coefficients are also validated according to the experimental results in Tan *et al.* (2014). In this study, the reflection coefficient is defined as $K_r = A_r/A_i$, in which A_i and A_r are the incident and reflected wave amplitudes measured at wave gauges G2 and G3, respectively. In accordance with the wave amplitudes in the narrow gap, A_i and A_r are also the averaged wave amplitudes in the steady states between 100 - 200 seconds. As shown in Fig. 7, the minimal peak values of the reflection coefficients K_r can be observed by the present viscous numerical model, which is in good agreement with the observation in the experiments. The corresponding frequencies of the minimal peak values are equal to the resonant frequency of fluid oscillation in the narrow gap, indicating that the significant energy dissipation happens around the resonant condition. However, the potential flow results cannot capture the energy dissipation due to the assumption of inviscid fluid and irrotational flow, leading to the results of $K_r = 1$ at the scope of all the frequencies. Finally, the variations of K_r against ω predicted by the viscous numerical model are found to be in good agreement with the experimental data, confirming that the present numerical wave flume is capable of producing the acceptable results of reflection coefficients. More interestingly, the reflection coefficients by the viscous fluid flow model seem to be almost identical to the experimental results after the minimal value is reached (i.e. at the high-frequency range), but there is a little discrepancy at the low-frequency range. The low-frequency wave can generate more developed boundary layer, which may require much finer mesh around the body surface to capture accurately.

Validations for wave forces on the box are conducted against the semi-analytical and Boundary Element Method results by Tan *et al.* (2014), where the artificial damping was adopted for improving the accuracy of potential flow model. Besides, the linear potential flow solutions without the artificial damping are also utilized for comparisons. As shown in Fig. 8, the linear potential flow model over-predicts the wave forces on the box, demonstrating the indispensable of viscous fluid model. A little discrepancy between the results of present viscous model and improved potential flow mod-

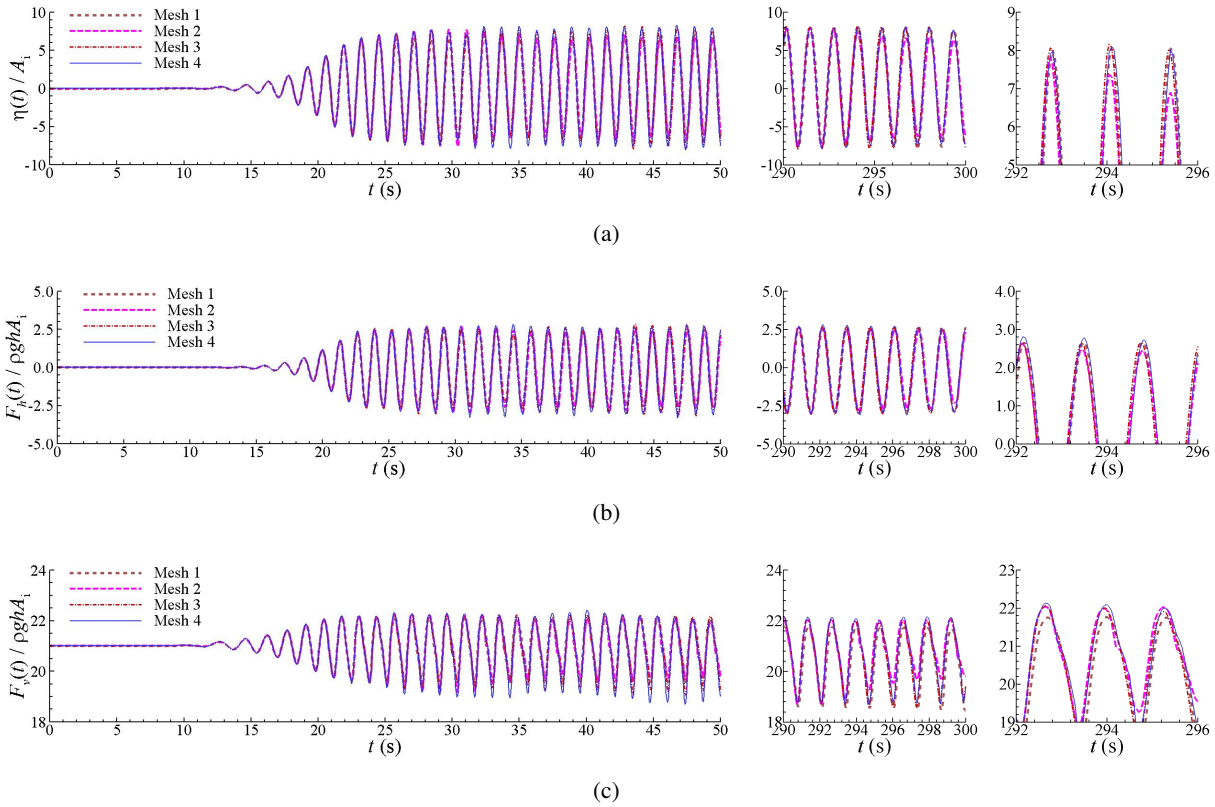

FIG. 3: Mesh convergent tests for the evolutions of wave responses in the narrow gap and wave forces on the box in the wave at resonant frequency with $A_i = 0.012$ m. (a) $\eta(t)/A_i$, (b) $F_h(t)/\rho g h A_i$, (c) $F_v(t)/\rho g h A_i$.

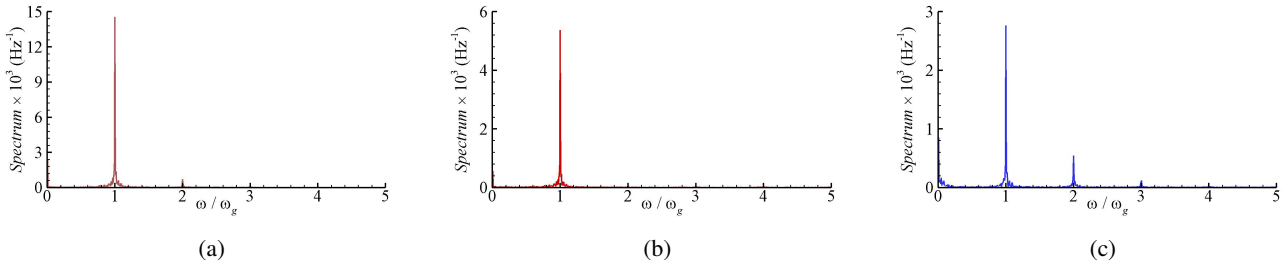

FIG. 4: Fourier analysis of wave responses in the narrow gap and wave forces on the box in the wave at resonant frequency with $A_i = 0.012$ m. (a) Wave response, A_g, (b) Horizontal force, F_h, (c) Vertical force, F_v

el by Tan *et al.* (2014) can be observed. The reason is that the values of artificial damping coefficients f and μ in Tan *et al.* (2014) are calibrated by the experimental data according to the free surface amplitude in the narrow gap. Generally speaking, the present numerical results are in agreement with both the improved semi-analytical and numerical solutions in Tan *et al.* (2014), indicating the present model can work well in predicating the wave forces on the box.

Finally, the first-order harmonic components of the horizontal and vertical wave forces are also included in Fig. 8, which are obtained by using the bandpass filtering approach for the steady-state evolutions between 100 - 200 seconds. Numerical simulations show the agreement between the total horizontal wave force and its first harmonic; while the magnitudes of higher harmonic components are remarkably smaller than that of the first harmonic. It again indicates the free surface nonlinearity is insignificant in the horizontal wave force for this case. As for the vertical wave force, the higher harmonic components become slightly more important, which is also reflected in the Fourier analysis in Fig. 4c. Generally speaking, the first harmonic component is dominating in both the horizontal and vertical wave forces on the box. This also agrees with the results for wave resonance between two fixed bodies in Gao *et al.* (2019).

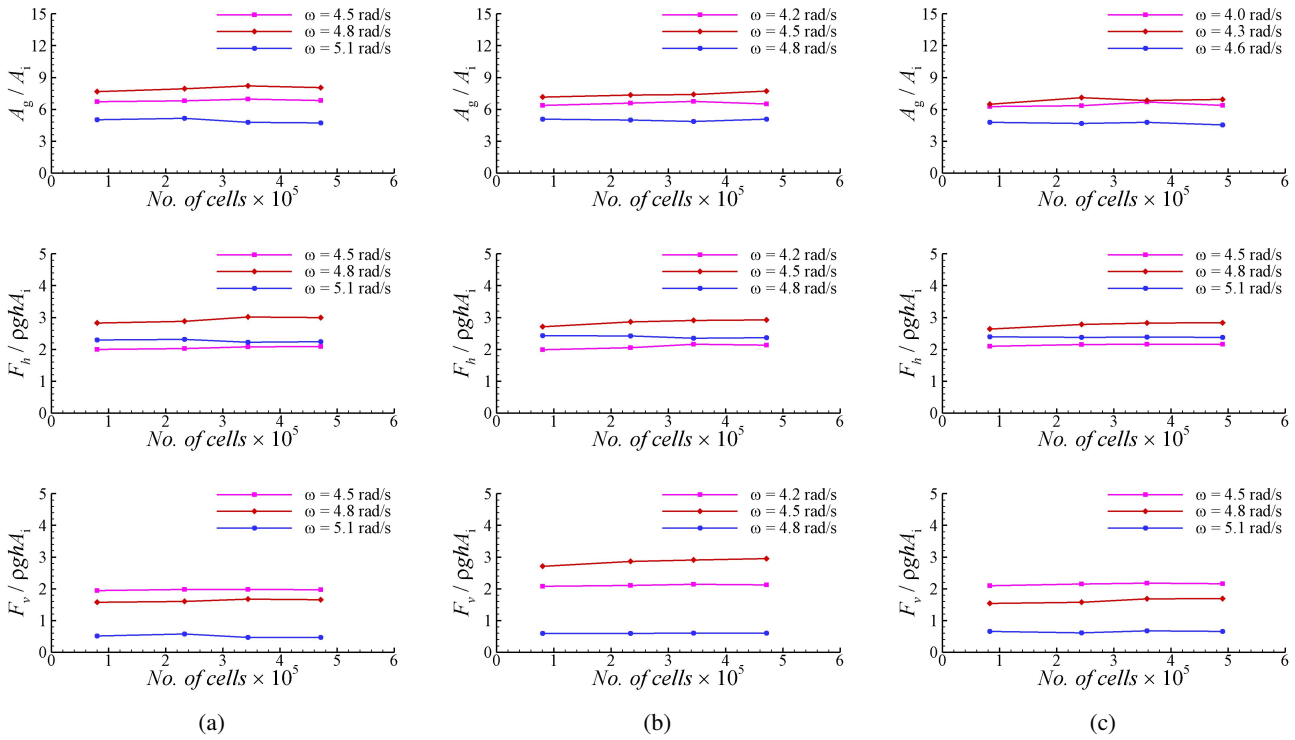

FIG. 5: Mesh convergent tests for the amplitudes of free surface oscillations in the narrow gap and wave forces on the box for various geometries at $A_i = 0.012$ m. (a) $B_g = 0.050$ m, $D = 0.252$ m, (b) $B_g = 0.070$ m, $D = 0.252$ m, (c) $B_g = 0.090$ m, $D = 0.252$ m.

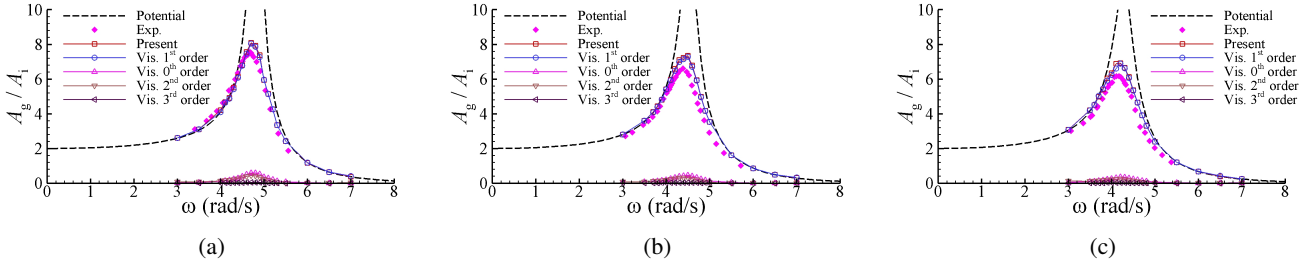

FIG. 6: Comparisons of normalized wave amplitudes A_g/A_i in the narrow gap for various configurations at $A_i = 0.012$ m. (a) $B_g = 0.050$ m, $D = 0.252$ m, (b) $B_g = 0.070$ m, $D = 0.252$ m, (c) $B_g = 0.090$ m, $D = 0.252$ m.

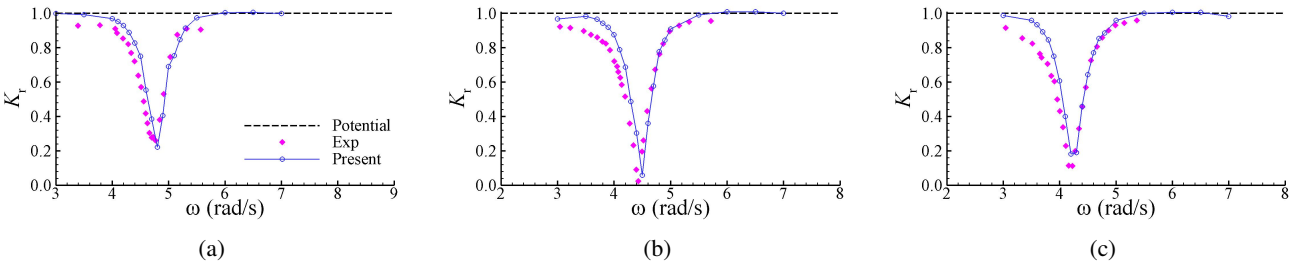

FIG. 7: Comparisons of reflection coefficients K_r for various configurations at $A_i = 0.012$ m. (a) $B_g = 0.050$ m, $D = 0.252$ m, (b) $B_g = 0.070$ m, $D = 0.252$ m, (c) $B_g = 0.090$ m, $D = 0.252$ m.

V. GENERAL DESCRIPTION OF PISTON-MODAL RESONANCE

The validation study in the previous section shows that the present viscous numerical model is able to reproduce well the studied scenario of gap resonance in the box-wall sys-

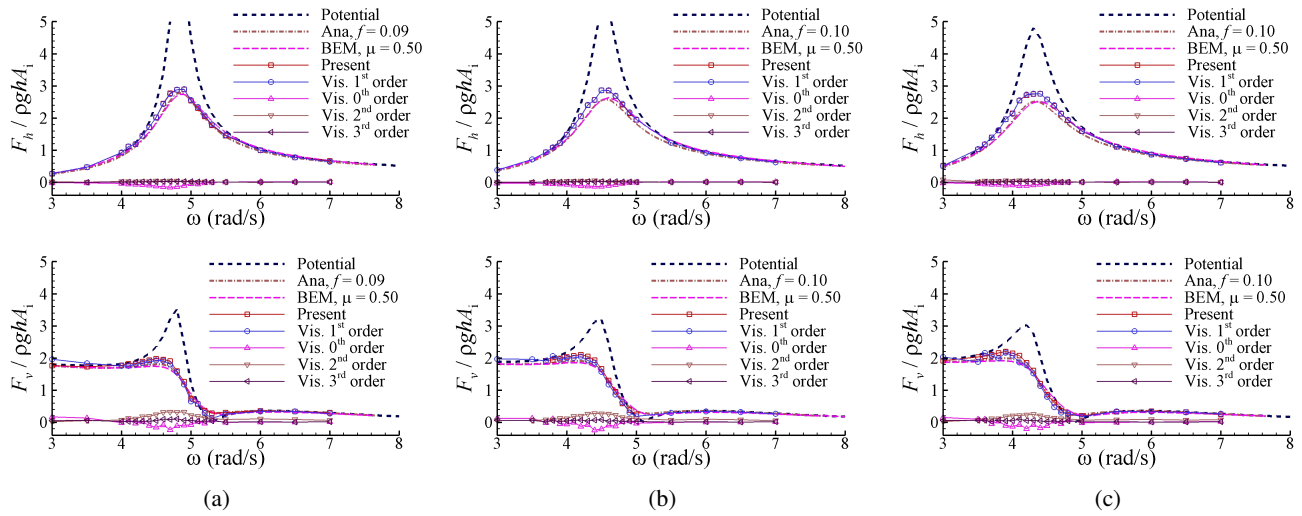

FIG. 8: Comparisons of the horizontal and vertical wave forces F_h and F_v on the box for various configurations at $A_i = 0.012$ m. (a) $B_g = 0.050$ m, $D = 0.252$ m, (b) $B_g = 0.070$ m, $D = 0.252$ m, (c) $B_g = 0.090$ m, $D = 0.252$ m

tem. It is adopted to investigate the wave responses and wave forces induced by the fluid resonance under wave actions. Our main objective is to study the influence of fluid viscosity and flow rotation on the behavior of piston-modal behavior. The variations of wave amplitudes in the narrow gap and in the upstream of the box A_g and A_u, the horizontal and vertical wave forces F_h and F_v, and the reflection coefficient K_r against the incident wave frequency ω are investigated, including the comparisons of the results between potential flow and viscous fluid flow models. For the purpose of shortening the length, only the geometry of $D = 0.252$ m under the incident wave amplitude $A_i = 0.012$ m is considered. The scope of incident wave frequency ω is from 0.1 to 8.0 rad/s in the linear potential flow model; while the viscous fluid flow model mainly focuses on the range of resonant conditions.

Numerical explanations begin with the free surface oscillations in the vicinity of the box-wall system, that is, wave amplitudes in the narrow gap and in the upstream of the box, as shown in Fig. 9. Potential flow model can firstly manifest a general impression for the variation of wave amplitude with incident wave frequency. Around the resonant frequency, the free surface amplitude in the narrow gap (measured by wave gauge G1 located in the middle of the gap, A_g/A_i) approaches to the maximal peak value; while the minimal peak value can be observed in the upstream of the box (measured by wave gauge G4 located at 0.005 m upstream of the box, A_u/A_i). This is the process of energy transformation of local near-field wave-wave and wave-body interactions during the piston-modal resonance in the box-wall system. When the incident wave frequency is close to the resonant frequency, the large-amplitude piston-type of fluid oscillation can be excited, and the energy is required to support the resonant fluid motion in the narrow gap. This energy comes from the incident wave, leading to the decrease of wave amplitude in the upstream of the box around the resonant frequency. On the other hand, the large-amplitude fluid oscillation in the narrow gap can be taken as a radiation source, which can result in the increase of wave amplitude in the upstream of the box. Therefore, a little discrepancy on the corresponding frequencies between the maximal and minimal peak values in the wave amplitudes at G1 and G4 can be observed in these figures. It is also the process of local energy transformation, where the energy is from inside to outside of the gap in the form of radiation.

The potential flow results can only express a general understanding on the behavior of wave responses; while the real physical phenomena of wave responses around the resonant condition should be simulated by the viscous fluid flow model. The essential assumption of the potential flow model is the fluid inviscid and flow irrotational. According to the comparisons between the potential flow and viscous fluid flow results, the influence of fluid viscosity and flow rotation on the behavior of piston-modal resonance can be investigated. Numerical results in Fig. 9 suggest that the resonant wave amplitude at wave gauge G1 is over-predicted significantly by the potential flow model, indicating that the energy dissipation due to the fluid viscosity and rotational motion can reduce the free surface oscillation in the narrow gap around the resonant frequency. Oppositely, the wave amplitude at wave gauge G4 around the resonant frequency is under-estimated by the potential flow model, implying that the fluid viscosity and rotational motion are able to increase the wave response in the upstream of the box. Energy dissipation mainly occurs in the vicinity of the gap, leading to the decrease of wave amplitude in the narrow gap. Correspondingly, less wave energy is required to support the oscillation of resonant fluid, and more wave energy can retain in the upstream of the box. This is the reason for the increase of wave amplitude in the upstream of the box, where the change of energy transformation associated with free surface motion is the essential mechanism behind the phenomenon. Further comparison shows that the corresponding frequencies between the maximal and minimal peak values of the wave amplitudes at G1 and G4 by the viscous

fluid flow model approach to the same with each other. The decrease of radiation wave by the fluid oscillation in the narrow gap is the reason for this result, which is essentially due to the energy dissipation.

According to the comparisons between two numerical models mentioned above, a three-phase variation of wave amplitudes with incident wave frequency can be suggested, that is, low frequency range, medium frequency range (around resonant frequency), and high frequency range. The potential flow model is able to work well at the scopes of low and high frequency ranges, indicating the fluid viscosity and flow rotation is ignorable. However, the influence of fluid viscosity and flow rotation cannot be neglected in the region of medium frequencies, especially around the resonant frequency. On one hand, the energy dissipation can result in the decrease of resonant amplitude in the narrow gap, directly. On the other hand, the change of energy transformation can lead to the increase of wave amplitude in the upstream of the box, which in fact is the influence of energy dissipation, indirectly. This is a real physical phenomenon relating to the local near-field wave-wave and wave-body interactions induced by the piston-modal resonance. The dynamic mechanism behind it is the interaction between the energy dissipation induced by the fluid vortical flow and energy transformation associated with free surface motion.

Fig. 10 depicts the comparisons of horizontal and vertical wave forces on the box obtained by the potential flow and viscous fluid flow models. It can be observed that the definition of the three-phase variation for wave amplitude in the narrow gap is also suitable for the wave forces on the box. The close relationship between the free surface oscillation in the narrow gap and the wave forces on the box can be adopted to explain the similarity. The maximal horizontal wave forces can be observed around a particular frequency, which is denoted as the resonant frequency of wave forces, corresponding to the counterpart of resonant frequency of free surface oscillation in the narrow gap. According to the comparisons between Figs. 9 and 10, we can observe that the resonant frequency of F_h is always larger than that of A_g in viscous fluid flow results. The influence of wave response in the upstream of the box is the main reason for this discrepancy. Distinct to the viscous fluid flow model, the exaggerated wave amplitude in the narrow gap has the dominant effect on the horizontal wave force in potential flow results, and consequently lead to that the maximal wave force always occurs at the resonant frequency of fluid oscillation in the narrow gap. This is not the real physical behavior because the ignorance of fluid viscosity and flow rotation under the potential flow assumption.

Variations of vertical wave force on the box with incident wave frequency ω are also depicted in Fig. 10. The vertical wave force on the box decreases gradually with ω in the region of low wave frequency. At the range of medium frequencies, the vertical force F_v has a small increase, and then decreases rapidly with incident wave frequency. The noticeable peak values at the resonant frequency in potential flow solutions even disappear in viscous fluid flow results. It indicates that the energy dissipation by vortical motion has dramatical effect on the vertical wave force. The potential flow model even fails to predict the variation trends of the vertical wave force with incident wave frequency. A lowest vertical wave force F_v locating at the frequency bound higher than the resonant frequency can be observed in potential flow solutions. It is a fictional response frequency by the potential flow model, where the corresponding F_v is under-estimated.

Numerical investigations are also extended to the reflection coefficient of box-wall system, as shown in Fig. 11. Due to the total reflection phenomenon in the box-wall system under the wave action, the reflection coefficient K_r in fact can express the process of energy dissipation. Potential flow model predicts the results of $K_r = 1$ in all the scope of incident wave frequencies, which is in agreement to the law of energy conservation. In viscous fluid flow results, dramatical decrease of reflection coefficient can be observed around the resonant frequency, indicating the energy dissipation due to the fluid viscosity and rotational motion. Further comparisons indicate that the corresponding frequency of minimal reflection coefficient is the same with the resonant frequency of wave amplitude in the narrow gap, confirming that the largest piston-type free surface oscillation in the narrow gap can generate the most significant energy dissipation in the fluid field.

VI. INFLUENCE OF INCIDENT WAVE AMPLITUDE

Special attention is paid to the influence of incident wave amplitude on the behavior of piston-modal resonance, concerning with incident wave frequency. Numerical results of wave amplitudes for the geometry of D = 0.252 m at three incident wave amplitudes, A_i = 0.004 m, 0.008 m, 0.012 m, are illustrated in Fig. 12. Again, the linear potential flow solutions are included in the numerical analysis for the purpose of comparison. It can be observed that the significant effect of incident wave amplitude is mainly in the medium frequency range, especially around the resonant frequency. For a specific geometry, the normalized free surface amplitude in the narrow gap decreases with the increase of incident wave amplitude. More relative energy dissipation by fluid viscosity and flow rotation in the vicinity of the narrow gap at resonant conditions can lead to the phenomenon. However, the normalized wave amplitude at wave gauge G4 increases with the increase of incident wave amplitude, implying that more relative wave energy retains in the upstream of the box. Summarizing the variation tendency mentioned above, we can obtain that the increase of incident wave amplitude can result in the viscous fluid flow results being deviated more from the potential flow results. This means the influence of fluid viscosity and flow rotation on the wave responses around the box is more important for larger incident wave amplitude, including the energy dissipation in the gap region and the energy transformation between the inside and outside of the box. As for the resonant frequency, comparisons in Fig. 12 suggest that it is hardly affected by the incident wave amplitude/or the resonant amplitude in the narrow gap in present numerical simulations.

Fig. 13 shows the magnitudes of horizontal and vertical wave forces F_h and F_v on the box under different incident wave amplitudes. Again, the significant effect of incident wave am-

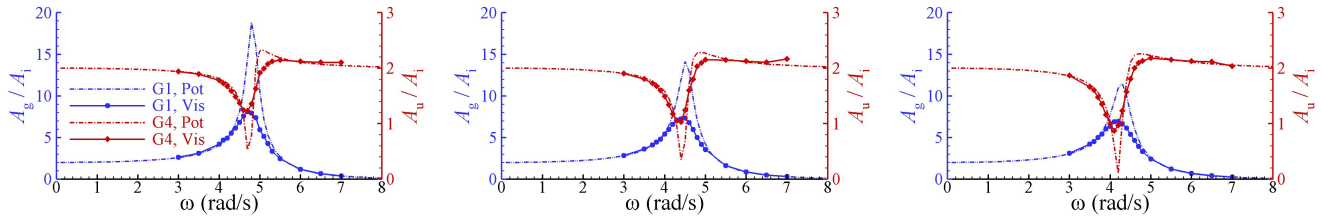

FIG. 9: General description for the wave amplitudes in the narrow gap and in the upstream of the box by the potential flow and viscous fluid flow models. (a) B_g = 0.050 m, D = 0.252 m, (b) B_g = 0.070 m, D = 0.252 m, (c) B_g = 0.090 m, D = 0.252 m.

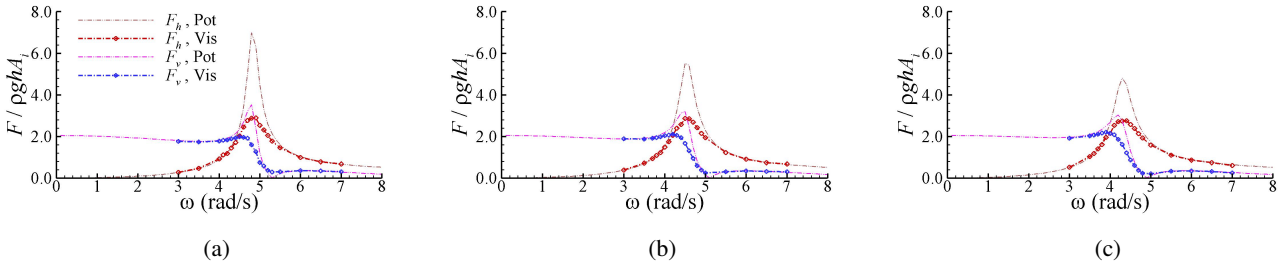

FIG. 10: General description for the horizontal and vertical wave forces by the potential flow and viscous fluid flow models. (a) B_g = 0.050 m, D = 0.252 m, (b) B_g = 0.070 m, D = 0.252 m, (c) B_g = 0.090 m, D = 0.252 m.

plitude can be observed in the region of medium wave frequencies. If the incident wave frequency is outside a certain band at either side of the resonant frequency, the insignificant influence of incident wave amplitude on the wave forces can be observed. Numerical simulations suggest that the normalized amplitude of the horizontal wave force $F_h/\rho ghA_i$ decreases with the increase of incident wave amplitude around the resonant frequency. It is similar to the variation of free surface oscillation in the narrow gap, implying that the energy dissipation in the vicinity of the gap is the dominating factor for that of horizontal wave force. As for vertical wave force, a two-phase variation at the scope of medium frequencies can be suggested. The decrease of normalized vertical wave force $F_v/\rho ghA_i$ with the increase of incident wave amplitude can be observed around the resonant frequency; while the increase of normalized vertical wave force $F_v/\rho ghA_i$ can be observed at the frequency bound higher than the resonant frequency, where the $F_v/\rho ghA_i$ approaches to zero in the potential flow simulations. Referring to the Bernoulli equation, the vertical wave force is closely relevant with the flow velocity under the box bottom. Many factors can affect the velocity flow field under the box bottom, including the shedding structure and eddy motion, which can lead to the complex variations of velocity flow. Analogous with the wave responses, the wave forces, including the horizontal and vertical wave forces, are influenced more by the fluid viscosity and flow rotation, which increase with the increase of incident wave amplitude. Finally, the incident wave amplitude also hardly affect the resonant frequency of wave forces in present numerical results.

The influence of incident wave amplitude on the behavior of reflection coefficient K_r is considered in Fig. 14. The dramatical decrease of the reflection coefficients can be observed for three incident wave amplitudes at the resonant frequency, implying significant energy dissipation happens. However, in difference to the resonant wave amplitude and wave forces results, there is no uniform rules on the variations of reflection coefficient with incident wave amplitude for different box-wall configurations. A typical example could be cited that the increased reflection coefficient can be observed in Fig. 14a, implying less percent of energy dissipation happens with the increase of incident wave amplitude. Oppositely, the decrease of reflection coefficient with the increase of incident wave amplitude can be found in Fig. 14c, indicating the larger incident wave amplitude can lead to relatively more energy dissipation. Roughly speaking, there are two factors affecting the variation of reflection coefficient: one is the reflection by the upstream of box; and the other is the energy dissipation in the narrow gap. The increase of incident wave amplitude tends to enlarge the reflection wave from the upstream of box, and hence relatively less wave energy can enter into the narrow gap of the box-wall system. It tends to amplify the reflection coefficient by the larger incident wave amplitude at the resonant frequency. On the other hand, the larger incident wave amplitude can lead to larger resonant wave response and more significant energy dissipation in the narrow gap, which reduces the reflection coefficient at the resonant frequency. The opposite effect by the above factors is the main reason for the complex hydrodynamic behavior of the reflection coefficient in Fig. 14. Furthermore, the above results can also indicate that the energy dissipation is not the only factor to affect the behavior of

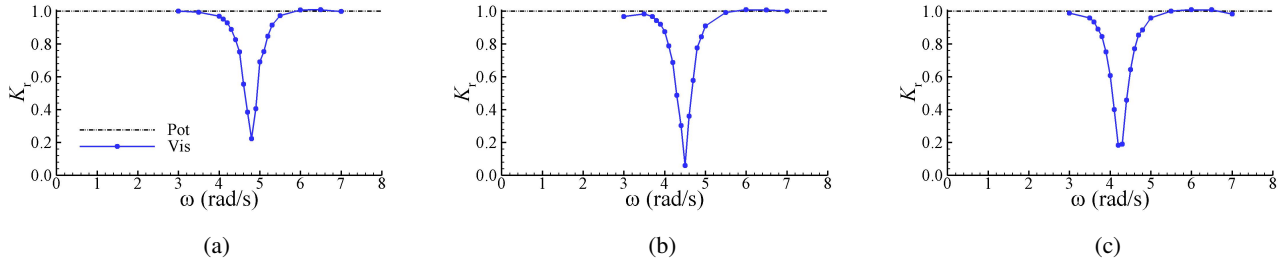

FIG. 11: General description for reflection coefficients by the potential flow and viscous fluid flow models. (a) B_g = 0.050 m, D = 0.252 m, (b) B_g = 0.070 m, D = 0.252 m, (c) B_g = 0.090 m, D = 0.252 m.

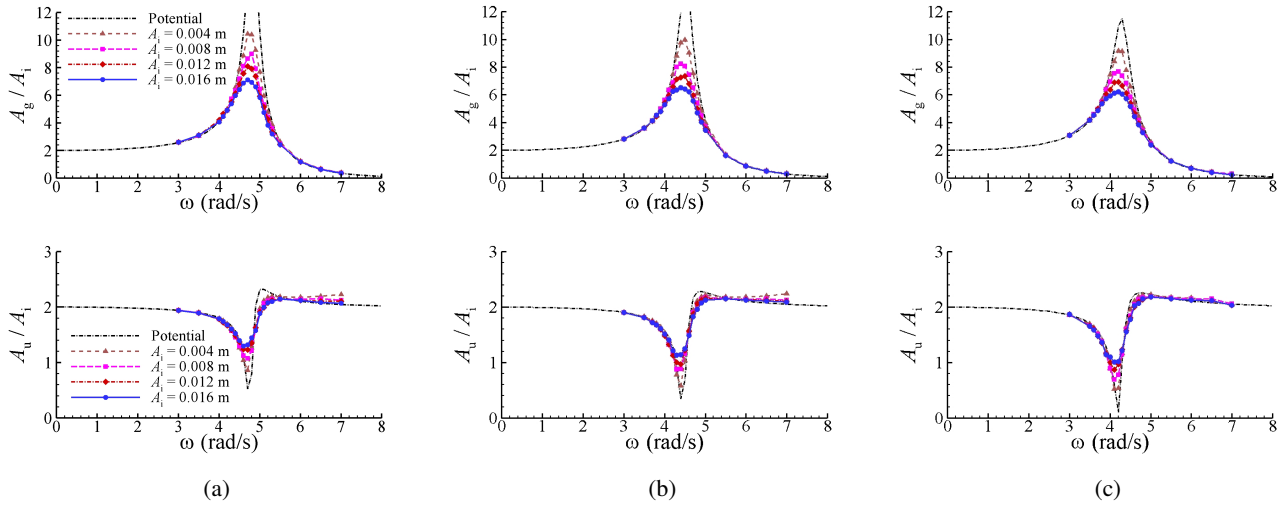

FIG. 12: Comparisons of normalized wave amplitudes A_g/A_i and A_u/A_i in the narrow gap and in the upstream of the box under various incident wave amplitudes. (a) B_g = 0.050 m, D = 0.252 m, (b) B_g = 0.070 m, D = 0.252 m, (c) B_g = 0.090 m, D = 0.252 m.

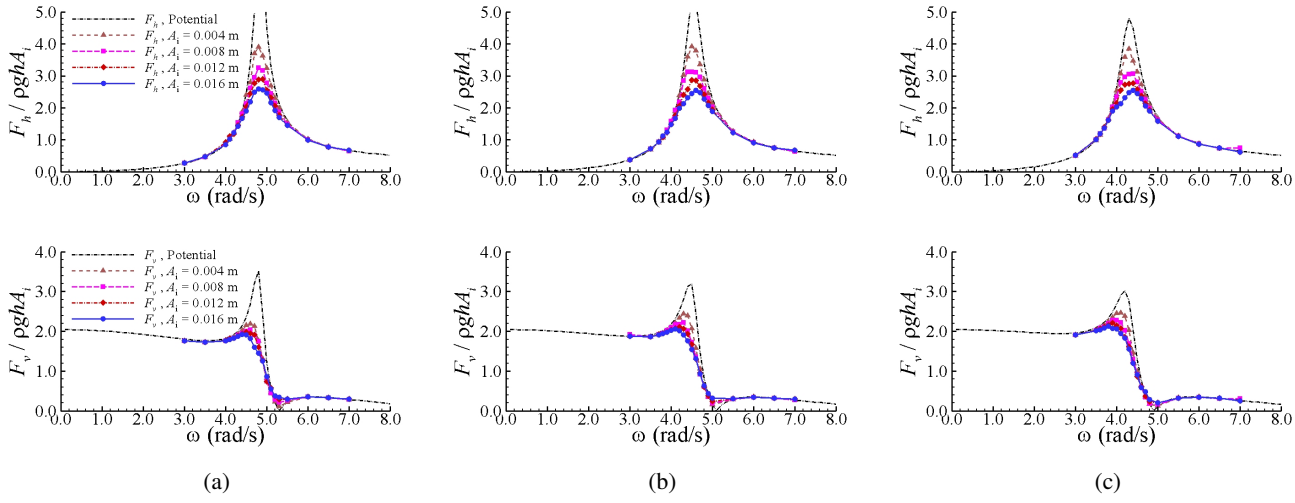

FIG. 13: Comparisons of normalized horizontal and vertical wave forces $F_h/\rho g h A_i$ and $F_v/\rho g h A_i$ on the box under various incident wave amplitudes. (a) B_g = 0.050 m, D = 0.252 m, (b) B_g = 0.070 m, D = 0.252 m, (c) B_g = 0.090 m, D = 0.252 m.

piston-modal resonance.

VII. INFLUENCE OF THE GAP BREADTH AND BOX DRAFT

In this section, the dependence of piston-modal behavior on the gap breadth and box draft is investigated. All of the geometries under the incident wave amplitude A_i = 0.012 m are simulated. Figs. 15 and 16 show the variations of wave amplitudes with gap breadth and box draft, respectively. Numerical simulations suggest that the resonant frequency of free surface oscillation in the narrow gap tends to decrease with the increase of gap breadth and box draft. Based on the motion equation of a linear-spring-mass system for the free surface oscillation, the decrease of resonant frequency can be understood because more fluid mass is entrapped by the larger gap breadth or box draft. As for the resonant amplitude, it is believed that the piston-modal free surface oscillation has closely relevant with the volume of fluid entering into the narrow gap from the gap entrance. The injected water volume, defined by Δ, during half period can be evaluated as follows,

$$\Delta = \int_0^{\frac{T}{2}} \int_{x_l}^{x_r} v(x,t)\,dx\,dt = B_g \int_0^{\frac{T}{2}} \tilde{v}(t)\,dt \tag{6}$$

where x_l and x_r are the left and right ends of the gap bottom, respectively. T is the incident wave period and $v(x,t)$ is the vertical velocity component of fluid flow. $\tilde{v}(t) = \frac{1}{x_r - x_l}\int_{x_l}^{x_r} v(x,t)\,dx$ is the time-dependent space-averaged vertical velocity along cross-section of gap bottom. In accordance with the free surface amplitude in the narrow gap, the amplitude of $\tilde{v}(t)$ in the steady state between 100 - 200 seconds is averaged as the amplitude of time-dependent space-averaged vertical velocity, defined as V_g. More specifically, the piston-modal resonant wave amplitude should be proportional to the relative injected water volume per gap breadth,

$$A_g \propto \frac{\Delta}{B_g} = \frac{1}{B_g}\int_0^{\frac{T}{2}} \int_{x_l}^{x_r} v(x,t)\,dx\,dt = \int_0^{\frac{T}{2}} \tilde{v}(t)\,dt \tag{7}$$

Eq. (6) shows that the injected water volume is relevant to gap breadth, resonant period, and vertical velocity; while Eq. (7) indicates that the resonant amplitude in the narrow gap should be controlled by resonant period and vertical velocity.

The calculated injected water volumes Δ and relative injected water volumes $\frac{\Delta}{B_g}$ for various box drafts and gap breadths at their respective resonant frequencies are tabulated in Tab. II. For a specific gap breadth, the increased Δ and $\frac{\Delta}{B_g}$ can be observed with the increase of box draft, which is analogous with the variation of resonant amplitudes in Fig. 16. By comparing the values of T and V_g in Tab. II, we can see that although V_g increases and then decreases with box draft D, the sustained increase of T can be observed. The increase of resonant period (or the decrease of resonant frequency) may be the essential reason for the increase of injected water volume and resonant amplitude with the increase of box draft. The calculated data in Tab. II also illustrates the influence of gap breadth on the injected water volume and wave amplitude at resonant frequency. Although the increase of injected water volume Δ can be observed with the increase of gap breadth, the decrease of relative injected water volumes $\frac{\Delta}{B_g}$ is able to result in the decrease of resonant amplitude in the narrow gap, which is similar with the influence of gap breadth on wave amplitude in Fig. 15. It is essentially due to the decrease of vertical velocity along the gap bottom $\tilde{v}(t)$, which is expressed as V_g in Tab. II. Furthermore, the magnitudes of the relative injected water volumes $\frac{\Delta}{B_g}$ and the wave heights in the narrow gap H_g ($H_g = 2A_g$) are almost identical with each other. The coincidence between them can be demonstrated under the assumption of harmonic functions. By substituting the linearized vertical velocity $\tilde{v}(t) = V_g \sin\omega t$ into Eq. (7), the following relationship can be obtained,

$$\begin{aligned}\frac{\Delta}{B_g} = \int_0^{\frac{T}{2}} \tilde{v}(t)\,dt &\approx V_g \int_0^{\frac{T}{2}} \sin\omega t\,dt \\ &\approx \omega A_g \int_0^{\frac{T}{2}} \sin\omega t\,dt = 2A_g = H_g\end{aligned} \tag{8}$$

where a relationship of $V_g = \omega_g A_g$ is utilized, which has been reported in Lu *et al.* (2010). The correlation between $\frac{\Delta}{B_g}$ and H_g can confirm that the free surface oscillation in the narrow gap is essentially controlled by the resonant frequency and the vertical velocity along the bottom.

Figs. 15 and 16 also illustrate the wave amplitude in the upstream of the box at wave gauge G4. A general comparison suggests that the wave amplitudes A_u/A_i decrease and increase with the increase of gap breadth and box draft, respectively, which is similar with the tendency of the wave amplitude in the narrow gap at wave gauge G1. The decrease of wave amplitude A_u/A_i in Fig. 15 means that more wave energy is absorbed to support the large-amplitude fluid oscillation and significant energy dissipation in the narrow gap with the increase of gap breadth. This is analogous with the increase of injected water volume Δ with the increase of gap breadth at the resonant frequency in Tab. II. As for the influence of box draft, the increase of piston-like free surface oscillation in the narrow gap can lead to the increase of radiation action, resulting in the increase of wave amplitudes A_u/A_i in the upstream of the box in Fig. 16.

Numerical simulations in Figs. 17 and 18 depict the influence of gap breadth and box draft on the horizontal and vertical wave forces F_h and F_v on the box, respectively. Analogous with the resonant frequency of the wave response in the narrow gap, the characteristic/resonant frequency tends to decrease with the increase of gap breadth and box draft, indicating that the large-amplitude piston-modal free surface oscillation in the narrow gap is the controlling factor on the behavior of wave forces. Generally, the variations of horizontal wave force with gap breadth and box draft are also the same with the wave amplitude in the narrow gap. It can be understood that the horizontal wave force is dependent on the wave responses around the box, in which the extremely wave amplitude in the narrow gap is the most significant factor. A little difference between them can also be observed, such as in Fig. 17a,

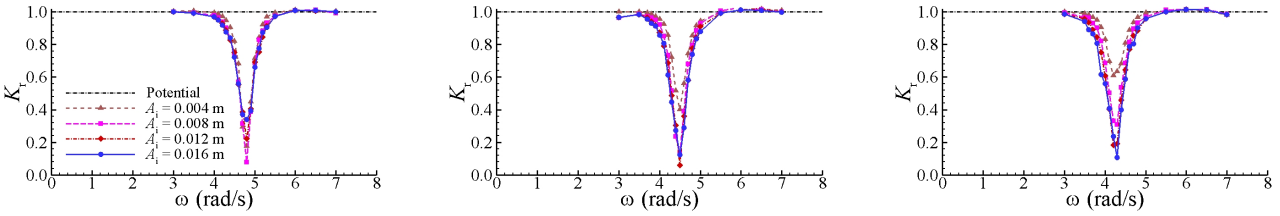

FIG. 14: Comparisons of reflection coefficients K_r under various incident wave amplitudes. (a) B_g = 0.050 m, D = 0.252 m, (b) B_g = 0.070 m, D = 0.252 m, (c) B_g = 0.090 m, D = 0.252 m.

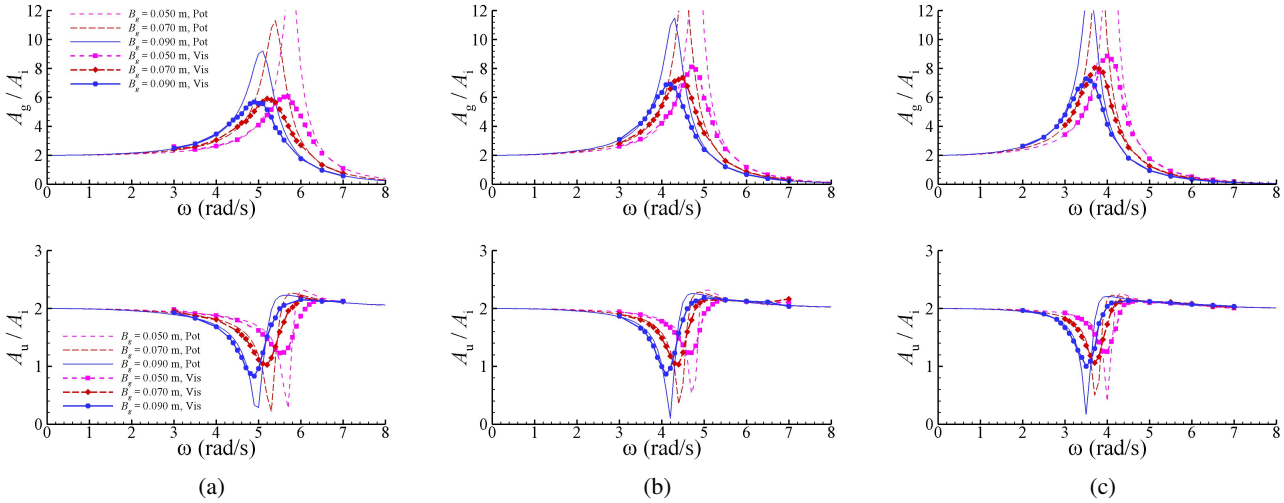

FIG. 15: Comparisons of wave amplitudes in the narrow gap and in the upstream of the box for various gap breadths. (a) D = 0.153 m, (b) D = 0.252 m, (c) D = 0.350 m.

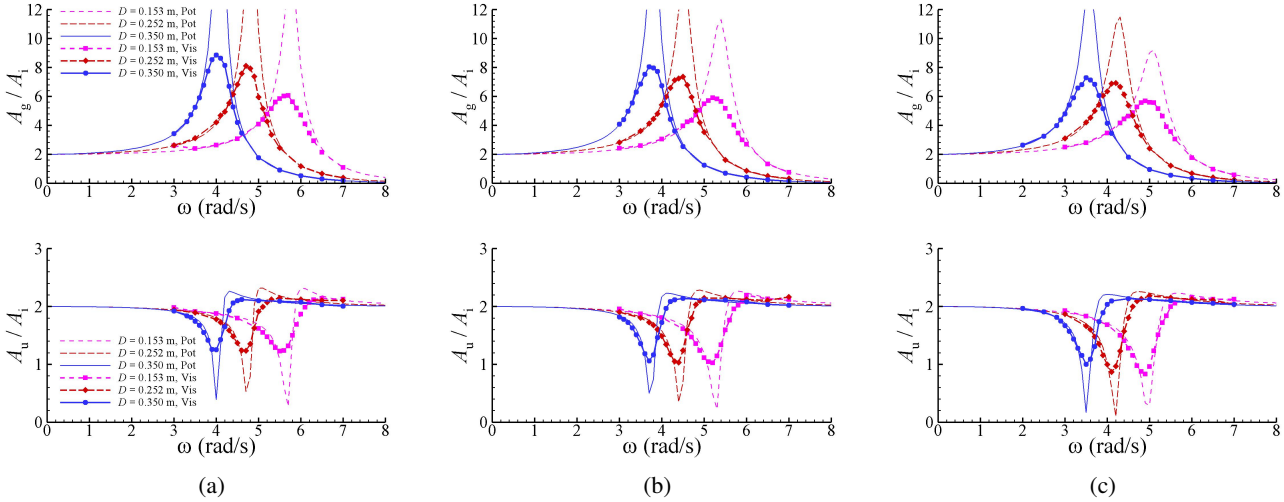

FIG. 16: Comparisons of wave amplitudes in the narrow gap and in the upstream of the box for various box drafts. (a) B_g = 0.050 m, (b) B_g = 0.070 m, (c) B_g = 0.090 m.

TABLE II: Water volume entering into the gap for various gap breadth and box draft at resonant conditions under incident wave amplitude $A_i = 0.012$ m

B_g (m)	D (m)	T (s)	V_g (m/s)	Δ (m^2)	$\frac{\Delta}{B_g}$ (m)	H_g (m)
0.050	0.153	1.102	0.384	6.74×10^{-3}	0.135	0.139
0.050	0.252	1.337	0.423	9.01×10^{-3}	0.180	0.184
0.050	0.350	1.571	0.399	9.98×10^{-3}	0.200	0.211
0.070	0.153	1.208	0.345	9.29×10^{-3}	0.133	0.136
0.070	0.252	1.396	0.371	11.54×10^{-3}	0.165	0.167
0.070	0.350	1.698	0.346	13.09×10^{-3}	0.187	0.195
0.090	0.153	1.282	0.319	11.72×10^{-3}	0.130	0.132
0.090	0.252	1.496	0.332	14.22×10^{-3}	0.158	0.160
0.090	0.350	1.848	0.257	14.31×10^{-3}	0.159	0.161

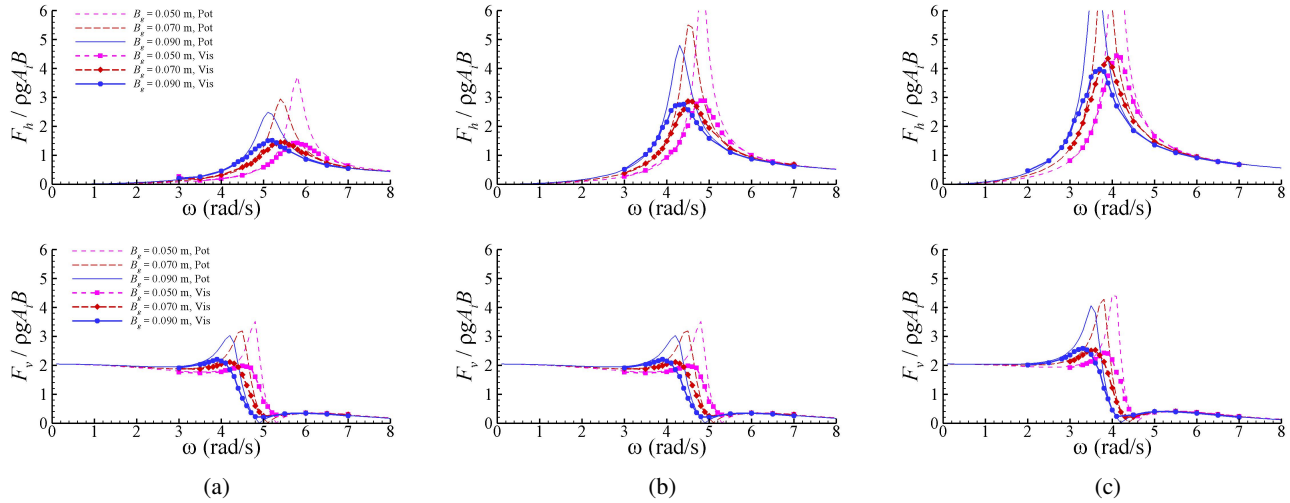

FIG. 17: Comparisons of horizontal and vertical wave forces on the box for various gap breadths. (a) $D = 0.153$ m, (b) $D = 0.252$ m, (c) $D = 0.350$ m.

where the increased resonant wave forces with the increase of gap breadth can be observed at $D = 0.153$ m. This can be explained by the wave response in the upstream of the box and velocity flow around the box, especially the vortex motion in the vicinity of the gap. The variation of vertical wave force with gap breadth and box draft, with regard to the incident wave frequency, is also considered in these figures. The increased vertical wave force can be observed with the increase of gap breadth and box draft if the incident wave frequency is smaller than the characteristic frequency in the medium frequency range. As for the regions of low and high frequencies, the insignificant effect of gap breadth and box draft on the horizontal and vertical wave forces can be observed, which can also be predicted by the potential flow model, correctly.

The reflection coefficients K_r for different gap breadths and box drafts against the incident wave frequency ω are depicted in Figs. 19 and 20. In accordance with the resonant frequency, the corresponding frequency of the minimal reflection coefficient can be observed to decrease with the increase of gap breadth and box draft. However, the variation of minimal peak value is not monotonic only increasing or decreasing with the change of gap breadth or box draft. As discussed in the previous section, many factors can affect the reflection coefficient, including the free surface oscillation in the narrow gap, the energy dissipation in the vicinity of the gap, the radiation action by the oscillating fluid bulk, etc. The increased gap breadth and box draft can result in more injected water volume in the narrow gap. On one hand, more wave energy is needed to support the oscillation of the fluid bulk, leading to the decrease of reflection coefficient. On the other hand, the oscillating fluid bulk can be taken as a radiation source, which generates a larger reflection coefficient. In addition, the energy dissipation connected with the vortical motion and the shielding effect associated with the geometries are also the indispensable factors. All these phenomena can lead to the complex hydrodynamic behavior of reflection coefficients with gap breadth and box draft in these figures.

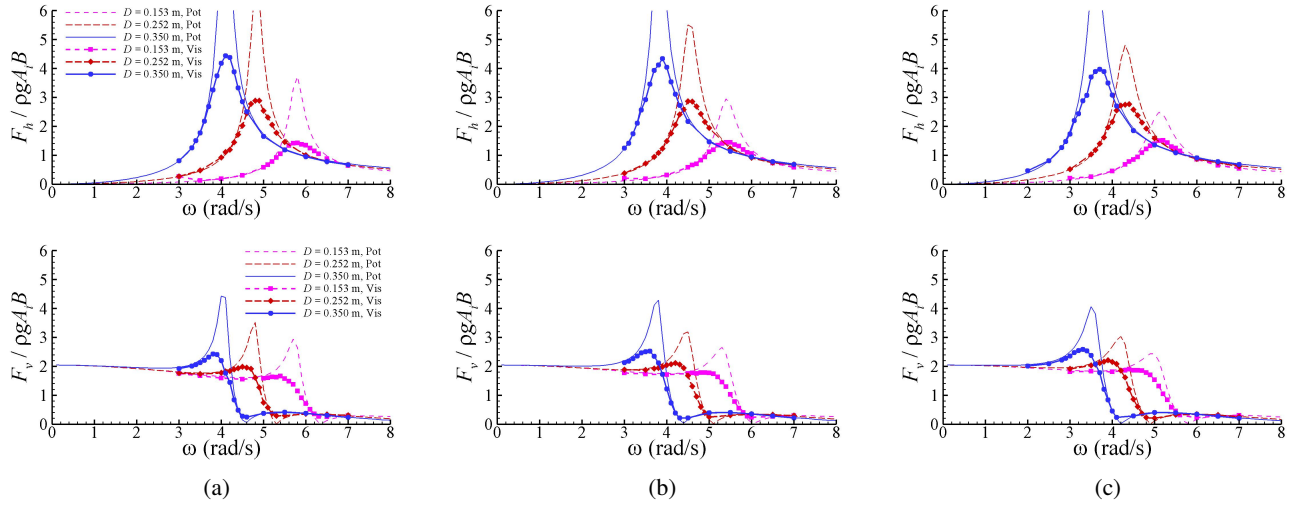

FIG. 18: Comparisons of horizontal and vertical wave forces on the box for various box draft. (a) B_g = 0.050 m, (b) B_g = 0.070 m, (c) B_g = 0.090 m.

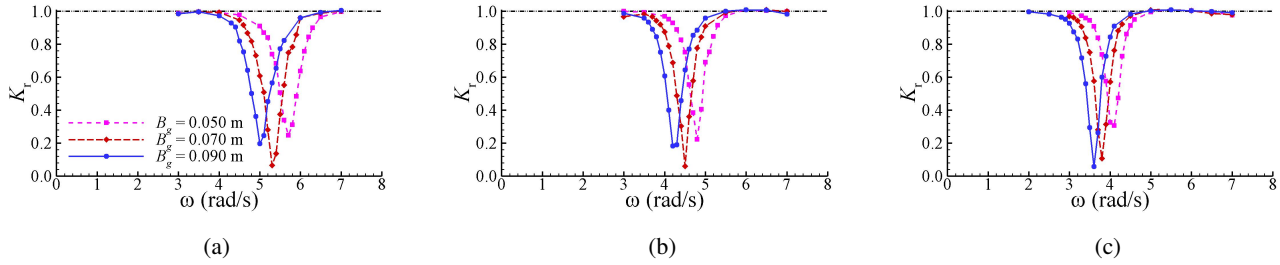

FIG. 19: Comparisons of reflection coefficients for various gap breadths. (a) D = 0.153 m, (b) D = 0.252 m, (c) D = 0.350 m.

VIII. VELOCITY FIELD PATTERN

The velocity field in the vicinity of the box-wall system is investigated for demonstrating the hydrodynamic behavior involved in the fluid resonance. The geometry of B_g = 0.050 m and D = 0.252 m with the incident wave amplitude A_i = 0.012 m and three incident wave frequencies, ω = 4.00, 4.70 and 5.30, are considered, where the frequencies adopted are the low, resonant and high frequencies, respectively. The velocity vectors together with vortices contours at eight time instants in a stable period T beginning from the up zero-crossing point of the piston-modal free surface oscillation in the narrow gap are depicted in Fig. 21, where the first, second and third rows are arranged corresponding to the sequence of incident frequencies mentioned above.

Roughly speaking, two typical flow modes can be identified in Fig. 21 corresponding to the resonant and non-resonant conditions. The flow evolutions at the resonant frequency, ω = 4.70, in the second row are investigated, firstly. At the beginning of free surface oscillation, there are three developed vortices in the vicinity of gap bottom, defined as $\{\mathbf{b}^-\}$, $\{\mathbf{a}^+\}$ and $\{\mathbf{a}^-\}$, respectively. The shear layers along the surfaces of the box and wall in the vicinity of the gap can be observed, and an attracted vortices $\{\mathbf{c}^+\}$ with positive sign is being generated from the edge profile of the box. The generating process is completed at the time instant of $t = 2T/8$. It is the time when the free surface in the narrow gap becomes the crest value, implying that the fluid begins to flow out of the narrow gap. The outflow of the fluid can lead to the outflow of the vortices $\{\mathbf{c}^+\}$, as shown in Fig. 21d. Meanwhile, a new negative vortex bubble $\{\mathbf{d}^-\}$ can be observed at the box lower corner beside the $\{\mathbf{d}^+\}$. Velocity field pattern indicates that the vortices $\{\mathbf{d}^-\}$ results from the strong flow shear, without the clear vortex structure identified by the flow vectors. With the time elapses, the vortices $\{\mathbf{d}^-\}$ is formed below the previous vortices $\{\mathbf{c}^+\}$, and another negative vortex bubble $\{\mathbf{c}^-\}$ is newly developed at the lower corner of the box. In difference to the vortices $\{\mathbf{d}^-\}$, the vortices $\{\mathbf{c}^-\}$ has the clear vortex structure, which can be identified by the flow vectors. After the time instant of $t = 5T/8$ in Fig. 21f, the vortices $\{\mathbf{d}^-\}$, $\{\mathbf{c}^+\}$ and $\{\mathbf{c}^-\}$ move downwards. A new positive vortices $\{\mathbf{e}^+\}$ begins to be generated at the time instant of $t = 7T/8$ in Fig. 21h. The initial flow scenery at $t = 0T$ can finally reappear at the time instant of $t = 1T$. According to the process of the velocity pattern during one period, the $P + S$ shedding mode can be suggested for the resonant condition. The sign 'P' refers to the pair of vortex bubble $\{\mathbf{c}^+\}$ and $\{\mathbf{c}^-\}$. The sign 'S' in-

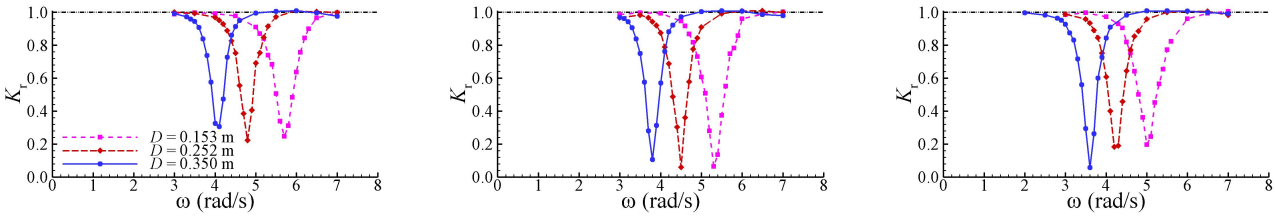

FIG. 20: Comparisons of reflection coefficients for various box drafts. (a) B_g = 0.050 m, (b) B_g = 0.070 m, (c) B_g = 0.090 m.

dicates the single vortex bubble $\{\mathbf{d}^-\}$ in these figures, which comes from the strong shear flow from the edge profile of the box by the velocity flowing out the gap.

The flow field patterns at the incident wave frequencies ω = 4.00 and 5.30 rad/s are presented in the first and third rows of Fig. 21, respectively. An general comparison suggests that the flow evolutions between the excitations of low and high frequencies are nearly the same to each other, which can be analyzed together. As shown in Fig. 21a, two developed vortices with opposite sign under the bottom of box can be observed, defined as $\{\mathbf{a}^+\}$ and $\{\mathbf{a}^-\}$, respectively. Another vortices $\{\mathbf{b}^+\}$ with positive sign is shedding from the edge profile of box. With the time elapses, the vortices $\{\mathbf{b}^+\}$ increases and falls off the inner corner of the narrow gap at $t = 2T/8$. Then, the flow begins to flow out of the gap, which leads to the vortices $\{\mathbf{b}^+\}$ propagating out of the narrow gap. Meanwhile, a new vortices $\{\mathbf{b}^-\}$ with negative sign is generated from the edge profile of the box at $t = 3T/8$. The flow vector identifies clearly the vortex structures of vortices $\{\mathbf{b}^-\}$. In the following half period, an inverse process can be observed. That is, the attached vortex $\{\mathbf{b}^-\}$ propagates out of the gap with the flow, and finally emerges with the secondary shear layer near the bottom of the box. Finally, the initial flow scenery at $0T$ reappears at T in this figure. By studying the flow pattern from the numerical simulations, the P shedding mode in the vicinity of the narrow gap can be suggested. The above P and P + S shedding modes can also be found in Vortex Induced Vibration (VIV) literature (Williamson and Govardhan, 2004; Zhao, Cheng, and Lu, 2014; Lu *et al.*, 2016; Munir *et al.*, 2018).

According to the analysis in this section, the vortex structures can be observed in all the cases with resonant and non-resonant frequencies. The strength of the vortices of the P + S shedding mode at resonant frequency is stronger than that of the P shedding mode at non-resonant frequencies, which is able to account for more significant physical dissipation in quality. The above phenomena can be understood according to a local Keulegan-Carpenter Number (KC Number), defined as $KC = V_g T/D$. The calculated KC Number are 1.20, 2.25 and 0.96 for ω = 4.00, 4.70 and 5.30, respectively. It can be observed that the maximal KC Number appears at the resonant frequency, indicating that the most significant vortical flow and energy dissipation happen. The above inference can also be demonstrated by the formula of dissipation rate (energy dissipation per unit volume and unit time). In the context of viscous fluid flow with incompressibility, the mechanical energy dissipation can be described by the dissipation rate from the energy equation $\Psi = 2\mu s_{ij}s_{ij}$ (Lamb, 1932), where μ stands for the dynamics viscosity and $s_{ij} = 0.5(u_{i,j} + u_{j,i})$ is the strain rate tensor. The function of dissipation rate can be re-formulated by subtracting the continuity equation as $\Psi = \mu[(v_{,x} - u_{,y})^2] + 4\mu(u_{,y}v_{,x} - u_{,x}v_{,y})$. For a wall bounded region, the total dissipation rate is mainly resulted from the enstrophy ($\widetilde{\Omega} = \Omega_i\Omega_i$, square of vortices), which is the first term of the above equation (Lu *et al.*, 2013). The above formula confirms that more significant dissipation can be generated by the stronger vortical motion at resonant frequency. Moreover, the flow pattern shows that the vortex structures shedding from the box are always near the gap bottom for the P + S shedding mode at resonant frequency; while the vortex structures are always far from the gap bottom and mainly below the box bottom for the P shedding mode at non-resonant frequencies. Reminding the conclusion in pervious section that the free surface amplitude in the narrow gap A_g is dependent on the vertical velocity along the gap bottom V_g, the significant influence of the P + S shedding mode on the piston-modal resonance in the narrow gap can be expected. Summarizing all the analysis mentioned above, we can confirm that the P + S shedding mode at resonant frequency is able to significantly affect the piston-like free surface oscillations in the narrow gap. Therefore, the influence of fluid viscosity and rotational flow cannot be neglected around resonant conditions. Therefore, the influence of fluid viscosity and rotational flow cannot be neglected around resonant conditions.

IX. CONCLUSION

The focus of the present work is on the wave resonance in the narrow gap formed by a rectangular box in front of a vertical wall. More specifically, the influence of fluid viscosity and flow rotation on the behavior of piston-modal wave resonance is investigated. This work is carried out by employing a viscous numerical wave flume based on the OpenFOAM® package, where three incident wave amplitudes with different frequencies at different gap breadths and box drafts are considered. The motivation of this study is to reveal the mechanical essence behind the piston-modal resonance from the perspective of interaction between energy dissipation and energy transformation. The major conclusions are given as follows,

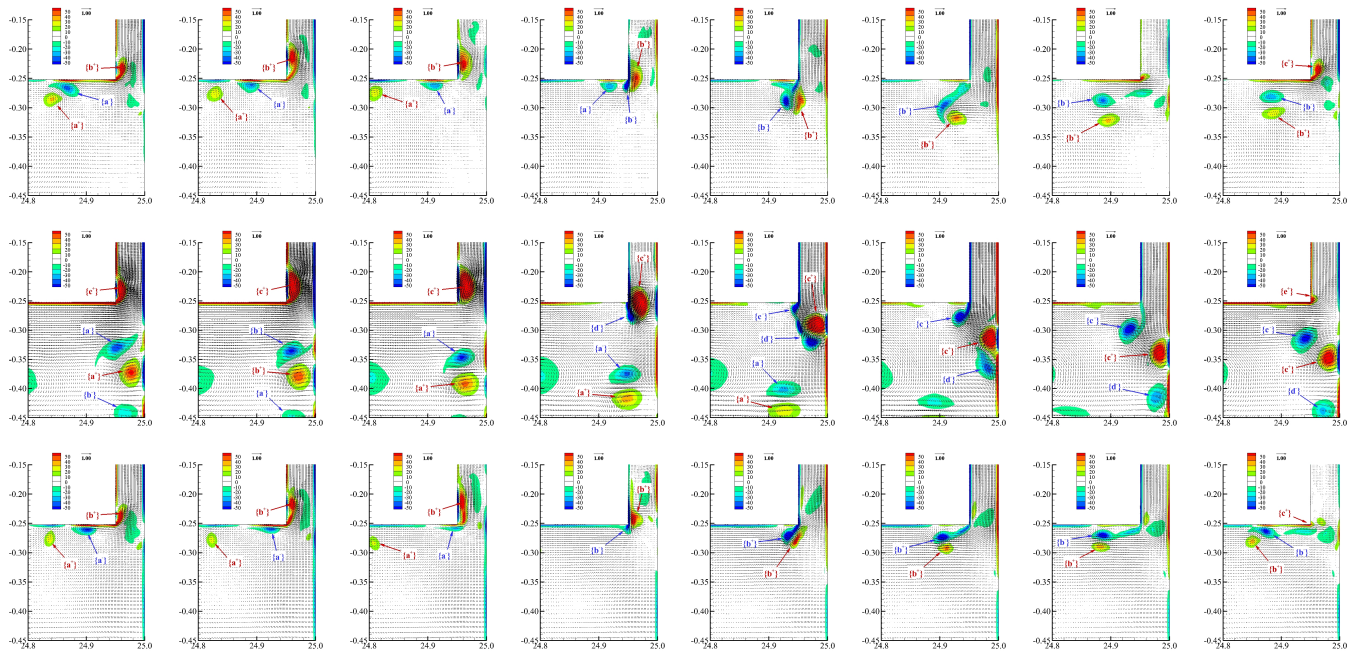

(a) (b) (c) (d) (e) (f) (g) (h)

FIG. 21: Velocity field and vortices contour in the nearby region of the gap entrance during one period of oscillating motion of fluid bulk in the narrow gap at various frequencies with $A_i = 0.012$ m for $B_g = 0.050$ m and $D = 0.252$ m. (a) $0T/8$, (b) $1T/8$, (c) $2T/8$, (d) $3T/8$, (e) $4T/8$, (f) $5T/8$, (g) $6T/8$, (h) $7T/8$
1st row: $\omega = 4.00$ rad/s; 2nd row: $\omega = 4.70$ rad/s; 3rd row: $\omega = 5.30$ rad/s

1) The large-amplitude piston-type free surface oscillation in the narrow gap can be observed around the resonant frequency. The harmonic analysis shows that the first harmonic wave component dominates the piston-modal free surface oscillation. Analogous phenomena can also be observed in the evolution of horizontal wave force. Only a little non-sinusoidal characteristic can be observed in the time signal of vertical wave force. Generally, the effect of free surface nonlinearity on the resonant behavior is insignificant when the incident wave frequency is close to the natural frequency of fluid bulk.

2) Around the resonant frequency, wave amplitudes in the narrow gap and in the upstream of the box are over-predicted and under-estimated by the potential flow model, respectively. The inherent neglect of energy dissipation due to the eddy motion and vortex shedding is the major reason for the over-prediction in the narrow gap. Meanwhile, the change of energy transformation between the inside and outside the box associated with free surface motion can lead to the under-estimation of the wave amplitude in the upstream of the box. In short, the influence of fluid viscosity and flow rotation not only leads to the decrease of free surface amplitude in the narrow gap, but also results in the increase of wave amplitude in the upstream of the box.

3) With increasing the incident wave amplitude, the normalized wave amplitude in the narrow gap become smaller around the resonant frequency. However, the increase of the normalized wave amplitude around the resonant frequency can be observed in the upstream of the box. The numerical results mentioned above can be summarized that the normalized wave amplitude around the box deviates more from the potential flow results with the increase of incident wave amplitude. It indicates that the influence of fluid viscosity and flow rotation on the wave responses is more significant with the increase of incident wave amplitude, including the energy dissipation in the gap region and energy transformation of local near-field interaction.

4) More fluid mass attends the resonance with the increase of gap breadth and box draft, leading to the decrease of resonant frequency of the fluid oscillation. The relation of equivalence between the piston-modal resonant amplitude and the relative injected water volume per gap breadth can be established, theoretically and numerically. Further analysis indicates that the piston-modal free surface amplitude is controlled by the resonant period and vertical velocity along the gap bottom. In the region of present study, the piston-modal resonant amplitudes in the narrow gap give rise to decrease and increase with the increase of gap breadth and box draft, respectively. The former is due to the decrease of vertical velocity along the gap bottom; while the latter is the reason of the increase of resonant period.

5) The definition of the three-phase variation for wave ampli-

tude in the narrow gap is also suitable for the wave forces on the box. With the increase of incident wave amplitude, the tendency of deviation of the potential flow results with the viscous fluid flow results can also be observed in the normalized wave forces. A minimal peak value of reflection coefficient at the resonant frequency can be observed by the viscous fluid flow model, indicating the significant energy dissipation happens in the whole fluid field. However, the dependence of the minimal reflection coefficient around the resonant frequency on the incident wave and box-wall geometry is quite complex.

6) Flow field examinations indicate that two typical flow modes, that is, the $P + S$ shedding mode and the $2P$ shedding mode, can be identified according to the resonant and non-resonant conditions, respectively. The vortical strength of the $P + S$ shedding mode is stronger than that of the P shedding mode, indicating more significant dissipation happens at the resonant frequency. Moreover, the vortex structures of the $P + S$ shedding mode are always near the gap bottom, which can further affect the wave amplitude in the narrow gap around the resonant frequency. The flow pattern analysis confirms the conclusion that the rotational flow plays an important role around the resonant frequency, which is highlighted for revealing the dynamic mechanism behind the piston-modal behavior in the box-wall system.

ACKNOWLEDGMENTS

This work was supported by the National Natural Science Foundation of China with Grant No. 51490673, the Fundamental Research Funds for the Central Universities with Grant No. DUT18LK09, and the Pre-research field Fund Project of the Central Military Commission of China with Grant No. 61402070201. The first author acknowledges the Supercomputer Center of Dalian University of Technology for providing computing resources.

Afshar, M. A., *Numerical wave generation in OpenFOAM*, Ph.D. thesis, Chalmers university of technology (2010).

Bonfiglio, L. and Brizzolara, S., "Amplitude induced nonlinearity in piston mode resonant flow: A fully viscous numerical analysis," Journal of Offshore Mechanics and Arctic Engineering **140**, 011101 (2018).

Chen, X.-B., "Hydrodynamics in offshore and naval applications-part i," in *Keynote lecture of 6th Intl. Conf. HydroDynamics, Perth (Australia)* (2004).

Engsig-Karup, A. P., *Unstructured nodal DG-FEM solution of high-order boussinesq-type equations* (MEK, 2006).

Faltinsen, O. M., *Sea loads on ships and offshore structures*, Vol. 1 (Cambridge university press, 1993).

Faltinsen, O. M., Rognebakke, O. F., and Timokha, A. N., "Two-dimensional resonant piston-like sloshing in a moonpool," Journal of Fluid Mechanics **575**, 359–397 (2007).

Feng, X. and Bai, W., "Wave resonances in a narrow gap between two barges using fully nonlinear numerical simulation," Applied Ocean Research **50**, 119–129 (2015).

Feng, X., Bai, W., Chen, X., Qian, L., and Ma, Z., "Numerical investigation of viscous effects on the gap resonance between side-by-side barges," Ocean Engineering **145**, 44–58 (2017).

Fredriksen, A. G., Kristiansen, T., and Faltinsen, O. M., "Experimental and numerical investigation of wave resonance in moonpools at low forward speed," Applied Ocean Research **47**, 28–46 (2014).

Fuhrman, D. R., Madsen, P. A., and Bingham, H. B., "Numerical simulation of lowest-order short-crested wave instabilities," Journal of Fluid Mechanics **563**, 415–441 (2006).

Gao, J. L., Zang, J., Chen, L. F., Ding, H. Y., and Liu, Y. Y., "On hydrodynamic characteristics of gap resonance between two fixed bodies in close proximity," Ocean Engineering **173**, 28–44 (2019).

Hirt, C. W. and Nichols, B. D., "Volume of fluid (vof) method for the dynamics of free boundaries," Journal of computational physics **39**, 201–225 (1981).

Huang, W., Li, B.-b., Chen, X.-b., and Araujo, R., "Numerical and experimental studies on dynamic gangway response between monohull flotel and fpso in non-parallel side-by-side configuration," Ocean Engineering **149**, 341–357 (2018).

Issa, R. I., "Solution of the implicitly discretised fluid flow equations by operator-splitting," Journal of computational physics **62**, 40–65 (1986).

Jacobsen, N. G., Fuhrman, D. R., and Fredsøe, J., "A wave generation toolbox for the open-source cfd library: Openfoam®," International Journal for Numerical Methods in Fluids **70**, 1073–1088 (2012).

Jasak, H., *Error analysis and estimation for the finite volume method with applications to fluid flows*, Ph.D. thesis, Imperial College London (University of London) (1996).

Jiang, S.-C., Bai, W., Cong, P.-W., and Yan, B., "Numerical investigation of wave forces on two side-by-side non-identical boxes in close proximity under wave actions," Marine Structures **63**, 16–44 (2019).

Jiang, S.-C., Bai, W., and Tang, G.-Q., "Numerical simulation of wave resonance in the narrow gap between two non-identical boxes," Ocean Engineering **156**, 38–60 (2018).

Kristiansen, T. and Faltinsen, O. M., "A two-dimensional numerical and experimental study of resonant coupled ship and piston-mode motion," Applied Ocean Research **32**, 158–176 (2010).

Lamb, H., *Hydrodynamics* (Cambridge university press, 1932).

Li, Z. F., Shi, Y. Y., and Wu, G. X., "Interaction of wave with a body floating on a wide polynya," Physics of Fluids **29**, 097104 (2017).

Liu, Y. and Li, H.-J., "A new semi-analytical solution for gap resonance between twin rectangular boxes," Journal of Engineering for the Marine Environment **228**, 3–16 (2014).

Liu, Y., Li, Y., Teng, B., Jiang, J., and Ma, B., "Total horizontal and vertical forces of irregular waves on partially perforated caisson breakwaters," Coastal Engineering **55**, 537–552 (2008).

Lu, L., Chen, X., Teng, B., Gou, Y., Jiang, S., and Guo, X., "Dissipation around rolling boxes," in *The 28th Int. Workshop on Water Waves and Floating Bodies, L'Isle sur la Sorgue, France* (2013).

Lu, L., Cheng, L., Teng, B., and Zhao, M., "Numerical investigation of fluid resonance in two narrow gaps of three identical rectangular structures," Applied Ocean Research **32**, 177–190 (2010).

Lu, L., Tang, G. Q., Liu, M. M., Chen, C. Q., and Xie, Z. H., "Numerical investigation of flow-induced rotary oscillation of circular cylinder with rigid splitter plate," Physics of Fluids **28**, 093604 (2016).

Lu, L., Teng, B., Cheng, L., Sun, L., and Chen, X., "Modelling of multibodies in close proximity under water waves-fluid resonance in narrow gaps," Science China Physics, Mechanics and Astronomy **54**, 16–25 (2011a).

Lu, L., Teng, B., Sun, L., and Chen, B., "Modelling of multi-bodies in close proximity under water waves-fluid forces on floating bodies," Ocean Engineering **38**, 1403–1416 (2011b).

Mayer, S., Garapon, A., Sørensen, L., *et al.*, "A fractional step method for unsteady free-surface flow with applications to non-linear wave dynamics," International Journal for Numerical Methods in Fluids **28**, 293–315 (1998).

Mei, C. C., *The applied dynamics of ocean surface waves*, Vol. 1 (World scientific, 1989).

Molin, B., "On the piston and sloshing modes in moonpools," Journal of Fluid Mechanics **430**, 27–50 (2001).

Moradi, N., Zhou, T., and Cheng, L., "Effect of inlet configuration on wave resonance in the narrow gap of two fixed bodies in close proximity," Ocean Engineering **103**, 88–102 (2015).

Munir, A., Zhao, M., Lu, L., and Z, N. D., "Three-dimensional numerical investigation of vortex-induced vibration of a rotating circular cylinder in

uniform flow," Physics of Fluids **30**, 053602 (2018).

Newman, J., "Progress in wave load computations on offshore structures," in *Invited Lecture, 23th OMAE Conference, Vancouver, Canada, http://www. wamit. com/publications* (2004).

Newman, J. N., *Marine hydrodynamics* (MIT press, 1977).

Ning, D., Su, X., Zhao, M., and Teng, B., "Hydrodynamic difference of rectangular-box systems with and without narrow gaps," Journal of Engineering Mechanics **141**, 04015023 (2015).

Ning, D.-Z., Zhu, Y., Zhang, C.-W., and Zhao, M., "Experimental and numerical study on wave response at the gap between two barges of different draughts," Applied Ocean Research **77**, 14–25 (2018).

Peric, M. and Swan, C., "An experimental study of the wave excitation in the gap between two closely spaced bodies, with implication for lng offloading," Applied Ocean Research **51**, 320–330 (2015).

Ren, K., Wu, G. X., and Thomas, G. A., "Wave excited motion of a body floating on water confined between two semi-infinite ice sheets," Physics of Fluids **28**, 127101 (2016).

Rusche, H., *Computational fluid dynamics of dispersed two-phase flows at high phase fractions*, Ph.D. thesis, Imperial College London (University of London) (2003).

Saitoh, T., Miao, G., and Ishida, H., "Theoretical analysis on appearance condition of fluid resonance in a narrow gap between two modules of very large floating structure," in *Proceedings of the Third Asia-Pacific Workshop on Marine Hydrodynamics, Shanghai, China* (2006) pp. 170–175.

Sun, L., Eatock Taylor, R., and Taylor, P. H., "Wave driven free surface motion in the gap between a tanker and an flng barge," Applied Ocean Research **51**, 331–349 (2015).

Tan, L., Lu, L., Liu, Y., Sabodash, O. A., and Teng, B., "Dissipative effects of resonant waves in confined space formed by floating box in front of vertical wall," in *The Eleventh ISOPE Pacific/Asia Offshore Mechanics Symposium* (International Society of Offshore and Polar Engineers, 2014).

Williamson, C. and Govardhan, R., "Vortex-induced vibrations," Annu. Rev. Fluid Mech. **36**, 413–455 (2004).

Zhang, X.-S. and Bandyk, P., "On two-dimensional moonpool resonance for twin bodies in a two-layer fluid," Applied Ocean Research **40**, 1–13 (2013).

Zhao, D.-y., Hu, Z.-q., and Chen, G., "Experimental investigation on dynamic responses of flng connection system during side-by-side offloading operation," Ocean Engineering **136**, 283–293 (2017).

Zhao, M., Cheng, L., and Lu, L., "Vortex induced vibrations of a rotating circular cylinder at low reynolds number," Physics of Fluids **26**, 413–455 (2014).

Zhao, W., Wolgamot, H. A., Taylor, P. H., and Eatock Taylor, R., "Gap resonance and higher harmonics driven by focused transient wave groups," Journal of Fluid Mechanics **812**, 905–939 (2017).